Metal Thin Films as SERS Substrates for the Detection of PAHs

by

© Mohammad Majibur Rahman

A Thesis submitted to the School of Graduate Studies

in partial fulfillment of the requirements for the degree of

Master of Science

Environmental Science

Faculty of Science

Memorial University of Newfoundland

MAY 2014

St. John's Newfoundland

Dedication

This thesis paper is dedicated to my beloved father

ABU BAKAR MIA

and son

MUNTASIR AHMAD MAHI

Abstract

Environmental pollution is a significant concern because of human and industrial discharges. Rapid and accurate detection of a pollutant is of the utmost importance in determining its health concern and environmental impact. This detection could be achieved through the development of a facile and hence broadly deployable sensor. In the present study, I was able to detect polycyclic aromatic hydrocarbons (PAHs) in aqueous solutions using a wide variety of mixed metal alloy Surface-enhanced Raman scattering (SERS) substrates. My work sought to optimize these substrates by varying their composition, base layers, and thermal annealing temperatures. Our findings have determined that the thinnest films, of the films I measured, exhibited the best SERS response. Furthermore, it was found that an annealing temperature of 300ºC was best able to produce the surface characteristics that lead to stronger signals. Finally, the base layer affected the results, silicon exhibited higher signals than glass.

Acknowledgements

I would like to express my profound gratitude and deepest sense of respect to my supervisor, Prof. Erika Merschrod, Department of Chemistry, for her able guidance and continuous inspiration during my course of study. Her cooperation and caring mentorship are the same qualities that I hope to bring to my future teaching career.

I would like to thank the members of my supervisory committee, Prof. Peter Pickup, Department of Chemistry, and Prof. Robert Davis, Department of Chemistry, for their support and suggestions.

The research would not have been accomplished without the help of my group members, especially Dmytro Grebennikov, Behrang Moazzez, Liam Whelan, and Brandon Furlong. My sincere gratitude belongs to all of them. Also, I am grateful to have been part of such a vibrant research group. The out-of-lab social events were especially enjoyable.

I am greatly indebted to Prof. Norm Catto (Chair, Environmental Science Program) and Prof. Joe Wroblewski (ex-chair, Environmental Science Program) for their help in keeping my program on schedule.

The service I received from the academic and administrative staff in the Department of Chemistry was beyond reproach. Their cooperation was very helpful.

I would like to thank the academic staff in the Department of Physics, especially Prof. Kris Poduska. She supported me during my research endeavors.

Special thanks are due to Ms Gail Kenny, Dean of Science Office, for assisting me whenever I required it.

I would like to thank Nicholas Button, Master of Environmental Science Candidate, for his proofreading of this manuscript.

I am grateful to the School of Graduate Studies for providing scholarship, Humber River Basin Project for supplying research materials, CFI and RDC for equipment facilities, AIF, ACOA, and PRNL for financial support in furnishing this research work.

Table of Contents

List of Figures

List of Table

List of Abbreviations

AFM	Atomic Force Microscope
EDX	Energy Dispersive X-ray
PAHs	Polycyclic aromatic hydrocarbons
ppm	Parts per million
QCM	Quartz Crystal Microbalance
RMS	Root-mean square
SEM	Scanning Electron Microscope
SERS	Surface-enhanced Raman scattering
EPA	Environmental Protection Agency
UV-vis	Ultraviolet-visible spectroscopy

Chapter 1

Introduction

1.1 Research background

It is well recognized that rapid industrialization poses a great threat to the very survival of Earth because it allows for the uncontrolled disposal of different wastes into the environment.[1,2] The excessive release of chemical contaminants into the environment can cause major public health problems and security problems.[3] Remediation of a contaminant requires an understanding of how much of it is present in a particular area.[1] This may be accomplished with a chemical sensor.[1,3] A chemical sensor consists of a transducer or a layer of chemical agents that are capable of transforming information into easily recognizable forms such as a change in voltage, change in current, or change in frequency. The change appears as a signal.[3] An ideal sensor should have good sensitivity, reproducibility, and stability.[4] In addition, it should be able to be used in both the laboratory and field.[5,6] Also, it should be inexpensive and allow for the non-destructive characterization of the sample in the ambient air.[6]

Even though there have been many technological advancements in the detection of environmental contaminants, the development of chemical sensors and biosensors that can quantify minute traces of contaminants in the presence of interfering agents has been

slow.[1] Most of the current techniques for monitoring organic contaminants in water such as chromatographic techniques or spectrometric techniques are time consuming and expensive.[1,6]

1.2 PAHs in the Environment

1.2.1 Origin of PAHs

Polycyclic aromatic hydrocarbons (PAHs) are a group of organic compounds that contain two or more fused benzene rings (Figure 1.2.1) in a linear or clustered arrangement.[7,8] They are a component of petroleum hydrocarbons and hence are important in energy production.[9] However, their worldwide distribution has caused concern because of their adverse effects on living organisms.[10,11] PAHs are ubiquitous compounds,[11] present in air,[12] water,[12] and sediments.[13] Soils are their principal sink.[8] Large amounts of PAHs enter the environment via the incomplete combustion of fossil fuels,[14] oil spills,[7] petrochemicals,[15] motor vehicles,[16] wood burning,[9] incinerations,[16] and pyrolysis of organic matter.[17] In sedimentary rocks and marine environments, high levels of PAHs are released by the biochemical transformations of small organic molecules.[18]

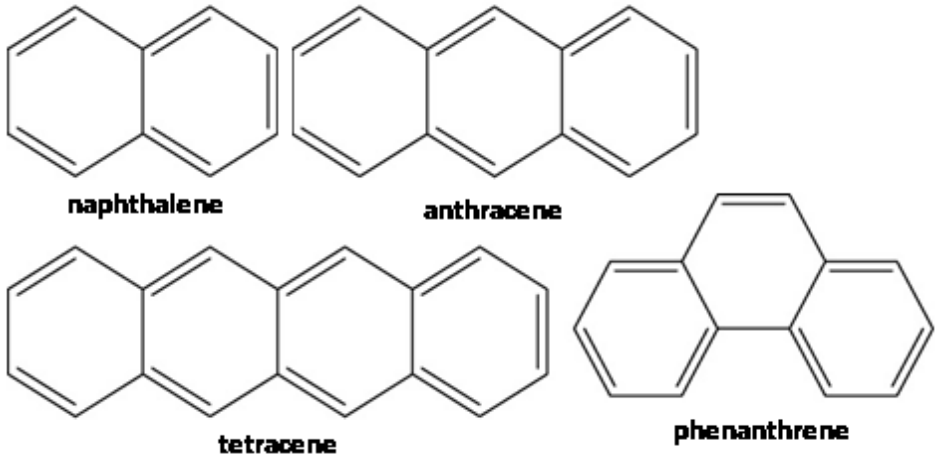

Figure 1.2.1: Structures of a few PAHs.[18]

1.2.2 Properties of PAHs

PAHs are hydrophobic,[8] but they exhibit strong affinity for lipids.[19] PAHs have dipole moments of zero or close to zero.[19] They do not show a tendency towards participating in different biodegradation processes and have relatively long lifetimes.[10,17] Even though there are hundreds of individual PAHs species,[7,15,17] the United States Environmental Protection Agency (US EPA) has classified sixteen PAHs as primary health hazards.[11,13,15,17] They are naphthalene, acenaphthene, acenaphthylene, fluorine, phenanthrene, anthracene, fluoranthene, pyrene, benz[a]anthracene, chrysene, benzo[b]fluoranthene, benzo[k]fluoranthene, benzo[a]pyrene, indeno[1,2,3-*cd*]pyrene, dibenz[*a,h*]anthracene, and benzo[*g,h,i*]perylene.[11] PAHs that have a low molecular weight as a consequence of their small number of aromatic rings (i.e. two to four) are less hydrophobic than those that have a high molecular weight.[11] All in all, the adverse effect

of PAHs on the aquatic environment is quite alarming; these are discussed in the next section.[20]

1.2.3 Health effects and detection of PAHs

PAHs are toxic to biota[10,21] and have an extremely hazardous nature.[22] They can cause mutagenic,[2,23] carcinogenic,[8,11] and teratogenic[20] effects on human body. It is observed in a recent study that the concentration of PAHs in surface seawater in the North Pacific and Arctic Ocean is in the range of 14 to 760 pg/L.[24] Therefore, sophisticated analytical tools are required for their detection.[21,25] The most common methods of identifying them in environmental samples are gas chromatography-mass spectrometry (GC-MS),[14] fluorescence spectroscopy,[23] and Resonance Raman spectrometry.[26] Mass spectrometry requires laborious sample preparation.[26] Fluorescence-based liquid chromatography can detect PAHs, but it is expensive and, like mass spectrometry, requires laborious sample preparation.[10] Also, it is affected by matrix problems such as spectral interference from other luminescent substances.[26] Moreover, the broad fluorescence bands from a mixture of PAHs overlap with many small peaks, thereby making their identification even more difficult.[26]

1.3 Raman spectroscopy for PAHs detection

1.3.1 Advantages of Raman spectroscopy

Raman spectroscopy is a promising technique for the detection of PAHs because it often provides an unambiguous sample characterization.[27] Raman spectroscopy is a non-destructive tool that produces 'fingerprints' of each species in a sample that can subsequently be used to identify that species, with even similar compounds showing distinct Raman spectra.[5,27,28] In addition, the technique allows for rapid sample characterization and minimal matrix preparation.[28] Raman bands are usually 10-100 times narrower than fluorescence bands, so this technique provides for multiple detection opportunities and causes only minor band overlap.[29] Also, Raman bands are not affected by humidity or the presence of oxygen.[29,30] This technique is suitable for bioimaging and remote sensing as well.[31]

1.3.2 Disadvantages of Raman Spectroscopy

Raman spectroscopy is an exceptional tool for the *in situ* identification of chemical contaminants,[20] but the identification of species at the ng/L level is difficult to accomplish with weak Raman signals.[27,32,33] An adsorbed surface layer usually contains 10^{12} to 10^{14} molecules per square cm, but ordinary Raman spectroscopy has a scattering cross-section on the order of 10^{-28} to 10^{-30} cm^2 per molecule per steradian.[34,35] This small scattering cross-section makes Raman spectroscopy unable to detect trace amounts of analytes.[10] In fact, a very high electromagnetic field enhancement is required for their detection.[34]

1.4 Detection of PAHs by SERS

1.4.1 A brief account of SERS

Surface-enhanced Raman scattering (SERS) is a vibrational spectroscopic technique[36,37] that produces the vibrational spectra of an analyte placed on a metal surface.[38,39,40] Fleischmann and his co-workers utilized SERS for the first time in the mid-1970s.[41,42,43,44,45] Using pyridine adsorbed to silver, they observed a Raman signal that was 6-orders of magnitude higher than the ordinary Raman signal.[41,45,46]

Nanostructures of noble metals that have relatively higher surface roughness are used extensively as SERS substrates.[45,47,48,49,50] Functionalized colloids of silver,[51,52] gold,[48,51] and copper[20,49] are SERS-active materials. Metal nanoparticle assemblies[53] and metal thin films[32] can serve as SERS substrates as well. In addition, transition metals such as Pt,[40,42,52] Co,[42,46] Rh,[40,42,46] Pd,[42,46,52] Ru,[46] Ni,[42,46] and alkali metals such as Li,[40,54] Na,[40,54] K,[40,54] Cs,[40] and Rb[40] are SERS-active materials. Also, the Raman signal-enhancing capabilities of semiconductors were observed by Yamada and Yamamoto.[42,55] However, insulators are SERS-inactive materials.[40]

1.4.2 Mechanism of SERS enhancement

There are three resonance models that contribute to the enhancement of a Raman signal by SERS: (i) surface plasmon resonances arising from the metal nanostructures, (ii) molecular resonances from the analyte molecule, and (iii) charge-transfer resonances involving the transfer of charge between the analyte and the metal surface.[39,56] However,

the two main mechanisms by which SERS enhances a Raman signal are the classical long-range electromagnetic field effect,[12,36,54,57,58] and the short-range chemical effect.[12,36,54,57,58] The simultaneous operation of these two effects increases molecular polarizability,[44,58,59] thereby enhancing the Raman signal so that it may be 10^{14}-10^{15} times higher than the ordinary Raman signal.[43,53,54,60] The electromagnetic field effect usually enhances the signal by a factor of 10^{8}-10^{10},[36,54,57] whereas the chemical effect usually enhances the signal by a factor of only 10^{1}-10^{2}.[36,54,57]

The enhancement of a Raman signal by SERS is attributable to the excitation of surface plasmons in the vicinity of the metal nanostructures.[59,61] The plasmons subsequently enhance the electromagnetic field around the metal nanostructures.[61,62] Raman intensity varies with the fourth power of the local field enhancement on metal surfaces,[63] therefore it allows to detect a very small amount of contaminants. However, the magnitude of a SERS enhancement depends on particle size of nanostructure materials,[64,65] particle shape,[65] geometry,[65] composition of materials,[65,66] surface morphology,[64,67] and the orientation of the target molecules.[61] The charge transfer between the roughened surface and the target species leads to a modification of the electronic properties of the molecules, thereby increasing its molecular polarizability.[44,62,68] The formation of a new charge transfer band leads to an amplification of Raman scattering cross-sections.[69,70]

1.4.3 Applications of SERS

SERS is a powerful spectroscopic technique,[56,71,72] that produces sharp molecular fingerprints[60,73] so as to allow non-destructive detection of adsorbed molecules.[10,74,75]

With the rapid development of nanotechnology, SERS is receiving more attention from scientists in the fields of chemistry,[45,76] physics,[76,77] biological detection,[10,37] and material sciences.[37] SERS detects structurally similar species in an aquatic environment with very little or no scattering interferences from water.[78,79] SERS can produce spectra from solid-gas, solid-liquid, and solid-solid interfaces.[40]

One important application of SERS is the detection of PAHs in aquatic environment. Sheng *et al.*[10] had prepared metal heterojunction materials by the deposition of Au particles inside the titania nanotubes to detect benzo(*a*)pyrene. The results revealed a significant SERS enhancement in quantifying the analyte. Pfannkuche *et al.*[20] carried out field monitoring of PAHs in the Baltic Sea using SERS and compared the results with those of GC/MS. It was observed that the two methods exhibited good performance in detecting as low as 150 ng/L of PAHs from sea water. Jiang *et al.*[56] synthesized silver nanoparticles on copper wire to detect PAHs from an aqueous phase. The results revealed that the silver based SERS substrates are very promising in developing sensors for the detection of contaminants in environmental samples.

The development of a facile and broadly deployable sensor for the *in situ* screening of surface water to detect the presence of PAHs has not been addressed so far. Hopefully, the as-prepared SERS sensor will lead to a greater interest in analytical monitoring of PAHs in areas of surface water pollution mediated by human intervention.[10,20,56]

1.5 Surface plasmons

1.5.1 Nature of surface plasmons

When irradiation strikes the surface of a metal, the conduction band electrons collectively oscillate at frequencies that are unique to the target metal.[80,81,82] The propagation of conduction band electrons induces local plasmonic resonance on the surface of the metal: surface plasmons are thus excited.[83,84,85,86] Surface plasmons may be referred to as surface plasmon polaritons[87,88] or plasma polaritons.[89] A strong plasmonic band appears when the frequency of the incoming electromagnetic radiation matches the resonance frequency of the conduction band electrons in the vicinity of the metal surface.[27,82]

1.5.2 Detection of surface plasmons

UV-vis spectroscopy is an excellent technique for identifying the plasmonic behaviour of metal particles.[90] However, metal particles can possess more than one plasmonic resonance band depending on their size,[91,92] shape,[91,92] surrounding media,[82,91] interparticle distance,[80,91] metal thickness,[38,93] geometry,[94] particle density,[95] surface morphology,[96] and the composition of target materials.[66] Also, the process of metal deposition and metal reduction can alter the position of a surface plasmon band.[97] For example, silver deposited by citrate borohydrate exhibits absorption bands within the 386 to 401 nm range[98] whereas silver nanoparticles deposited via thermal silver atoms that undergo subsequent nucleation exhibit absorption bands within the 453 to 548 nm range.[99] Also, silver reduced by ascorbic acid exhibits an absorption band at 480 nm.[99] In

practice, silver particles exhibit characteristic plasmonic peaks from 390 to 420 nm.[100] Localized surface plasmon resonance can cause the nanoparticles to absorb and scatter incident light to such an extent that a single particle could be viewed by an optical microscope in the UV-vis range of wavelengths.[75,101,102,103]

1.5.3 Importance of surface plasmons

In order to detect a harmful chemical species in an environmental sample, the detection technique must be selective for the target molecule.[104] In recent years, scientists have taken advantage of the surface features of metal nanostructures in the fields of optical sensing,[92,95,105] biological detection,[106,107,108] chemical analysis,[106,109] and surface-enhanced Raman spectroscopy.[85,92] One of the major features of noble metal nanostructures is their ability to enhance optical fields when certain molecules are placed on their surface.[63,110,111] Noble metals such as gold, silver, and copper possess unique linear and nonlinear optical properties,[58,62,66] large specific surface areas,[112,113] and high absorption cross-sections in the visible and infra-red regions of the electromagnetic spectrum.[97,114] Thin films of these metals have shown promise in being used as molecular sensors that can detect chemical contaminants like phenanthrene, benzo(a)pyrene, pyrene, etc.[90,115,116,117]

1.5.4 Surface plasmons and SERS hot spots

Most of the surface of a metal nanosubstrate is not SERS-active because the signal enhancement occurs within a very confined area.[118] The regions of the surface where the largest signal enhancements occur are called surface 'hot spots'.[118,119] The locations of 'hot

spots' can vary, but the interparticle junctions between two nanostructured aggregates are considered to be surface 'hot spots'.[43,54,57,90,118] A strong signal enhancement is observed with roughened surfaces of gold, silver, and copper because surface plasmon resonance occurs on the surface 'hot spots' in these metals.[46,54,74]

1.6 Motivations of the present work

Water pollution is increasing rapidly due to uncontrolled human interventions and industrial discharges.[1,2,3] It is necessary to detect PAHs in bodies of water because of their adverse effects on human health.[48] They must be detectable with a device that is rapid and inexpensive. The project described here aims to prepare noble metal-based SERS substrates for the detection of PAHs in water samples.

Bibliography

[1] Sarkar, T.; Gao, Y.; Mulchandani, A. *Appl. Biochem. Biotechnol.*, **2013**, 170, 1011-1025.

[2] Manzetti, S. *Poly. Aroma. Com.*, **2013**, 33, 311-330.

[3] Afzal, A.; Iqbal, N.; Mujahid, A.; Schirhagl, R. *Anal. Chimi. Acta*, **2013**, 787, 36-49.

[4] Shi, X.; Kwon, Y.-H.; Ma, J.; Zheng, R.; Wang, C.; Kronfeldt, H.-D. *J. Raman Spectrosc.*, **2013**, 44, 41-46.

[5] Ferrari, A. C.; Basko, D. M. *Nature Nanotech.*, **2013**, 8, 235-246.

[6] Sidek, O.; Quadri, S. A.; Kabir, S.; Afzal, M. H. B. *J. Experiment. Nanosci.*, **2013**, 8(2), 154-161.

[7] Nagy, A. S.; Szabó, J.; Vass, I. *J. Environ. Sci. Health: Part A*, **2013**, 48, 1190-1200.

[8] Jorfi, S.; Rezaee, A.; Mobeh-Ali, G.-A.; Jaafarzadeh, N. A. *Soil Sedi. Contamin.*, **2013**, 22, 890-911.

[9] Ball, A.; Truskewycz, A. *Environ. Sci. Pollut. Res.*, **2013**, 20, 4311-4326.

[10] Sheng, P.; Wu, S.; Bao, L.; Wang, X.; Chen, Z.; Cai, Q. *New J. Chem.*, **2012**, 36, 2501-2505.

[11] Liu, Y.-L.; Zhou, J.-B.; Zhao, R.-S.; Chen, X.-F. *Anal. Bioanal. Chem.*, **2012**, 404, 1603-1610.

[12] Xie, Y.; Wang, X.; Han, X.; Xue, X.; Ji, W.; Qi, Z.; Liu, J.; Zhao, B.; Ozaki, Y. *Analyst*, **2010**, 135, 1389-1394.

[13] Lin, C.; Liu, J.; Wang, R.; Wang, Y.; Huang, B.; Pan, X. *Soil Sedi. Contamin.*, **2013**, 22, 753-766.

[14] Du, J.; Jing, C. *J. Phys. Chem. C*, **2011**, 115, 17829-17835.

[15] Augusto, S.; Pereira, M. J.; Maguas, C.; Branquinho, C. *Chemosphere*, **2013**, 92, 626-632.

[16] McIntosh, A. D.; Fryer, R. J.; Webster, L.; Cundy, A. B. *J. Environ. Monit.*, **2012**, 14, 1335-1344.

[17] Nagy, A. S.; Simon, G.; Szabó, J.; Vass, I. *Environ. Monit. Assess.*, **2013**, 185, 4619-4631.

[18] Alajtal, A. I.; Edwards, H. G. M.; Elbagerma, M. A.; Scowen, I. J. *Spectrochimica Acta Part A*, **2010**, 76, 1-5.

[19] Obiri, S.; Cobbina, S. J.; Armah, F. A.; Naangmenyele, Z. *Environ. Sci. Pollut. Res.*, **2011**, 18, 1166-1173.

[20] Pfannkuche, J.; Lubecki, L.; Schmidt, H.; Kowalewska, G.; Kronfeldt, H.-D. *Marine Pollut. Bullet.*, **2012**, 64, 614-626.

[21] Kwon, Y.-H..; Ossig, R.; Hubenthal, F.; Kronfeldt, H.-D. *J. Raman Spectrosc.*, **2012**, 43, 1385-1391.

[22] Guerrini, L.; Garcia-Ramos, J. V.; Domingo, C.; Sanchez-Cortes, S. *Anal. Chem.*, **2009**, 81, 953-960.

[23] Qu, L.-L.; Li, Y.-T.; Li, D.-W.; Xue, J.-Q.; Fossey, J. S.; Long, Y.-T. *Analyst*, **2013**, 138, 1523-1528.

[24] Ma, Y.; Xie, Z.; Yang, H.; Möller, A.; Halsall, C.; Cai, M.; Sturm, R.; Ebinghaus, R. *J. Geophys. Res.: Atmos.*, **2013**, 118(11), 5822-5829.

[25] Bourgeault, A.; Gourlay-Francé, *Sci. Total Environ.*, **2013**, 454-455, 328- 336.

[26] Asher, S. A. *Anal. Chem.*, **1984**, 56, 720-724.

[27] Muniz-Miranda, M.; Gellini, C.; Giorgetti, E. *J. Phys. Chem. C*, **2011**, 115, 5021-5027.

[28] Robinson, A. M.; Harroun, S. G.; Bergman, J.; Brosseau, C. L. *Anal. Chem.*, **2012**, 84, 1760-1764.

[29] Xu, D.; Gu, J.; Wang, W.; Yu, X.; Xi, K.; Jia, X. *Nanotech.*, **2010**, 21, 375101 (1-8).

[30] Li, D.; Li, D.-W.; Fossey, J. S.; Long, Y.-T. *Anal. Chem.*, **2010**, 82, 9299- 9305.

[31] Lanin, A. A.; Fedotov, I. V.; Fedotov, A. B.; Sidorov-Biryukov, D. A.; Zheltikov, A. M. *Sci. Reports*, **2013**, 3, 1842 (1-5).

[32] Lucht, S.; Murphy, T.; Schmidt, H., Kronfeld, H.-D. *J. Raman Spectrosc.*, **2000**, 31, 1017-1022.

[33] Leverette, C. L.; Dluhy, R. A. *Colloids and Surfaces A: Physicochem. Eng. Aspects*, **2004**, 243, 157-167.

[34] Fan, M.; Andrade, G. F. S.; Brolo, A. G. *Anal. Chimi. Acta*, **2011**, 693, 7-25.

[35] Kudelski, A.; Wojtysiak, S. *J. Phys. Chem. C*, **2012**, 116, 16167-16174.

[36] Tripp, R. A.; Dluhy, R. A.; Zhao, Y. *Nanotoday*, **2008**, 3 (3-4), 31-37.

[37] Lin, H.-X.; Li, J.-M.; Liu, B.-J.; Liu, D.-Y.; Liu, J.; Terfort, A.; Xie, Z.-X.; Tian, Z.-Q.; Ren, B. *Phys. Chem. Chem. Phys.*, **2013**, 15, 4130-4135.

[38] Correia-Ledo, D.; Gibson, K. F.; Dhawan, A.; Couture, M.; Vo-Dinh, T.; Graham, D.; Masson, J.-F. *J. Phys. Chem. C*, **2012**, 116, 6884-6892.

[39] Londero, P. S.; Leona, M.; Lombardi, J. R. *Appl. Phys. Lett.*, **2013**, 102, 111101 (1-5).

[40] Duyne, R. P. V.; Hulteen, J. C.; Treichel, D. A. *J. Chem. Phys.*, **1993**, 99(3), 2101-2115.

[41] Otto, A.; Mrozek, I.; Grabhom, H.; Akemann, W. *J. Phys.: Condens. Matter*, **1992**, 4, 1143-1212.

[42] Jiang, L.; You, T.; Yin, P.; Shang, Y.; Zhang, D.; Guo, L.; Yang, S. *Nanoscale*, **2013**, 5, 2784-2789.

[43] Kim, K.; Choi, J.-Y.; Shin, K. S. *Spectrochimica Acta Part A*, **2013**, 100, 3-9.

[44] Péron, O.; Rinnert, E.; Lehaitre, M.; Crassous, P.; Compère, C. *Talanta*, **2009**, 79, 199-204.

[45] Campion, A.; Kambhampati, P. *Chem. Soc. Rev.*, **1998**, 27, 241-250.

[46] Li, J. F.; Tian, X. D.; Li, S. B.; Anema, J. R.; Yang, Z. L.; Ding, Y.; Wu, Y. F.; Zeng, Y. M.; Chen, Q. Z.; Ren, B.; Wang, Z. L.; Tian, Z. Q. *Nature Protoc.*, **2013**, 8(1), 52-65.

[47] Maznichenko, D.; Selvaganapathy, P. R.; Venkatakrishnan, K.; Tan, B. *Appl. Phys. Lett.*, **2012**, 101, 231602 (1-5).

[48] Tian, S.; Zhou, Q.; Gu, Z.; Gu, X.; Zheng, J. *Analyst*, **2013**, 138, 2604-2612.

[49] Bazzaoui, E. A.; Aubard, J.; Félidj, N.; Laurent, G.; Lévi, G. *J. Raman Spectrosc.*, **2005**, 36, 817-823.

[50] Tognalli, N.; Fainstein, A.; Calvo, E.; Bonazzola, C.; Pietrasanta, L.; Campoy-Quiles, M.; Etchegoin, P. *J. Chem. Phys.*, **2005**, 123, 044707 (1-9).

[51] Alvarez-Puebla, R. A.; Santos, D. S.; Aroca, R. F. *Analyst*, **2007**, 132, 1210-1214.

[52] Li, S.; Xu, P.; Ren, Z.; Zhang, B.; Du, Y.; Han, X.; Mack, N. H.; Wang, H.-L. *ACS Appl. Mater. Interfaces*, **2013**, 5, 49-54.

[53] Du, Y.; Liu, R.; Liu, B.; Wang, S.; Han, M.-Y.; Zhang, Z. *Anal. Chem.*, **2013**, 85, 3160-3165.

[54] Kim, K.; Lee, H. B.; Shin, K. S. *Spectrochimica Acta Part A*, **2013**, 100, 10-14.

[55] Yamada, H.; Yamamoto, Y. *Surf. Sci.*, **1983**, 134(1), 71-90.

[56] Jiang, X.; Lai, Y.; Yang, M; Yang, H.; Jiang, W.; Zhan, J. *Analyst*, **2012**, 137, 3995-4000.

[57] Kim, K.; Park, H. K.; Kim, N. H. *Langmuir*, **2006**, 22, 3421-3427.

[58] Kim, K.; Choi, J.-Y.; Lee, H. B.; Shin, K. S. *ACS Appl. Mater. Interfaces*, **2010**, 2(7),1872-1878.

[59] Prokopec, V.; Cejkova, J.; Matějka, P.; Hasal, P. *Surf. Interface Anal.*, **2008**, 40, 601-607.

[60] Aikens, C. M.; Madison, L. R.; Schatz, G. C. *Nature Photon.*, **2013**, 7, 508-510.

[61] Rout, C. S.; Kumar, A.; Fisher, T. S. *Nanotech.*, **2011**, 22, 395704 (1-8).

[62] Péron, O.; Rinnert, E.; Toury, T.; Chapelle, M. L.; Compère, C. *Analyst*, **2011**, 136, 1018-1022.

[63] Alonso-González, P.; Albella, P.; Schnell, M.; Chen, J.; Huth, F.; García- Etxarri, A.; Casanova, F.; Golmar, F.; Arzubiaga, L.; Hueso, L. E.; Aizpurua, J.; Hillenbrand, R. *Nature Commun.*, **2012**, 3, 684 (1-7).

[64] Qiu, H.; Zhang, Z.; Huang, X.; Qu, Y. *Chem. Phys. Chem.,* **2011**, 12, 2118-2123.

[65] Zhang, L.; Chen, L.; Liu, H.; Hou, Y.; Hirata, A.; Fujita, T.; Chen, M. *J. Phys. Chem. C*, **2011**, 115, 19583-19587.

[66] Fu, C. Y.; Kho, K. W.; Dinish, U. S.; Koh, Z. Y.; Malini, O. *J. Raman Spectrosc.*, **2012**, 43, 977-985.

[67] Roguska, A.; Kudelski, A.; Pisarek, M.; Lewandowska, M.; Dolata, M.; Janik-Czachor, M. *J. Raman Spectrosc.*, **2009**, 40, 1652-1656.

[68] Zheng, X.; Chen, Y.; Chen, Y.; Bi, N.; Qi, H.; Qin, M.; Song, D.; Zhang, H.; Tian, Y. *J. Raman Spectrosc.*, **2012**, 43, 1374-1380.

[69] Ojha, A. K.; Donfack, P.; Materny, A. *J. Raman Spectrosc.*, **2012**, 43, 1183-1190.

[70] Guerrini, L.; Garcia-Ramos, J. V.; Domingo, C.; Sanchez-Cortes, S. *Anal. Chem.*, **2009**, 81, 1418-1425.

[71] Huang, Z.; Meng, G.; Huang, Q.; Chen, B.; Zhu, C.; Zhang, Z. *J. Raman Spectrosc.*, **2013**, 44, 240-246.

[72] Jeon, H. C.; Park, S.-G.; Chao, S.; Yang, S.-M. *J. Mater. Chem.*, **2012**, 22, 23650-23654.

[73] Scholes, F. H.; Bendavid, A.; Glenn, F. L.; Critchley, M.; Davis, T. J.; Sexton, B. A. *J. Raman Spectrosc.*, **2008**, 39, 673-678.

[74] Li, J. F.; Huang, Y. F.; Ding, Y.; Yang, Z. L.; Li, S. B.; Zhou, X. S.; Fan, F. R.; Zhang, W.; Zhou, Z. Y.; Wu, D. Y.; Ren, B.; Wang, Z. L.; Tian, Z. Q. *Nature*, **2010**, 464, 392-395.

[75] Qian, X.; Peng, X.-H.; Ansari, D. O.; Yin-Geon, Q.; Chen, G. Z.; Shin, D. M.; Yang, L.; Young, A. N.; Wang, M. D.; Nie, S. *Nature Biotech.*, **2008**, 28(1), 83-90.

[76] Liu, J.-W.; Wang, J.-L.; Huang, W.-R.; Yu, L.; Ren, X.-F.; Wen, W.-C.; Yu, S.-H. *Sci. Reports*, **2012**, 2, 987 (1-7).

[77] Lu, G.; Li, H.; Liusman, C.; Yin, Z.; Wu, S.; Zhang, H. *Chem. Sci.*, **2011**, 2, 1817-1821.

[78] Bantz, K. C.; Haynes, C. L. *Vibra. Spectrosc.*, **2009**, 50, 29-35.

[79] Kahraman, M.; Zamaleeva, A. I.; Fakhrullin, R. F.; Culha, M. *Anal. Bioanal. Chem.*, **2009**, 395, 2559-2567.

[80] Chan, G. H.; Zhao, J.; Schatz, G. C.; Duyne, R. P. V. *J. Phys. Chem. C*, **2008**, 112, 13958-13963.

[81] Chahadih, A.; Hamzaoui, H. E.; Cristini, O.; Bigot, L.; Bernard, R.; Kinowski, C.; Bouazaoui, M.; Capoen, B. *Nano. Res. Lett.*, **2012**, 7, 487 (1-6).

[82] Zhang, X.; Zhang, J.; Wang, H.; Hao, Y.; Zhang, X.; Wang, T.; Wang, Y.; Zhao, R.; Zhang, H.; Yang, B. *Nanotech.*, **2010**, 21, 465702 (1-11).

[83] Zhang, F.; Zhang, L.; Mao, S.-C.; Chen, P.; Cui, J.-C.; Tang, Y.-G.; Wang, K.; Lin, L.; Qi, X.-D. *Environ. Technol.*, **2012**, 33(18), 2071-2075.

[84] McFarland, A. D.; Duyne, R. P. V. *Nano Lett.*, **2003**, 3(8), 1057-1062.

[85] Sherry, L. J.; Chang, S.-H.; Schatz, G. C.; Duyne, R. P. V.; Wiley, B. J.; Xia, Y. *Nano Lett.*, **2005**, 5(10), 2034-2038.

[86] Haes, A. J.; Chang, L.; Klein, W. L.; Duyne, R. P. V. *J. Am. Chem. Soc.*, **2005**, 127, 2264-2271.

[87] Miroshnichenko, A. E.; Kivshar, Y. S. *Science*, **2013**, 340, 283-284.

[88] Ozaki, M.; Kato, J.; Kawata, S. *Science*, **2011**, 332, 218-220.

[89] Kedem, O.; Tesler, A. B.; Vaskevich, A.; Rubinstein, I. *ACS Nano*, **2011**, 5(2), 748-760.

[90] Goh, M. S.; Lee, Y. H.; Pedireddy, S.; Phang, I. Y.; Tjiu, W. W.; Tan, J. M. R.; Ling, X. Y. *Langmuir*, **2012**, 28, 14441-14449.

[91] Tseng, M. L.; Huang, Y.-W.; Hsiao, M.-K.; Huang, H. W.; Chen, H. M.; Chen, Y. L.; Chu, C. H.; Chu, N.-N.; He, Y. J.; Chang, C. M.; Lin, W. C.; Hunag, D.-W.; Chiang, H.-P.; Liu, R.-S.; Sun, G.; Tsai, D. P. *ACS Nano*, **2012**, 6(6), 5190-5197.

[92] Jang, L.-W.; Jeon, D.-W.; Kim, M.; Jeon, J.-W.; Polyakov, A. Y.; Ju, J.-W.; Lee, S.-J.; Baek, J.-H.; Yang, J.-K.; Lee, I.-H. *Adv. Funct. Mater.*, **2012**, 22, 2728-2734.

[93] Jia, K.; Bijeon, J.-L.; Adam, P.-M.; Ionescu, R. E. *Plasmonics*, **2013**, 8, 143-151.

[94] Luther, J. M.; Jain, P. K.; Ewers, T.; Alivisatos, A. P. *Nature Mater.*, **2011**, 10, 361-366.

[95] Li, D.; Pan, L.; Li, S.; Liu, K.; Wu, S.; Peng, W. *J. Phys. Chem. C.*, **2013**, 117, 6861-6871.

[96] Lim, D.-K.; Jeon, K.-S.; Hwang, J.-H.; Kim, H.; Kwon, S.; Sun, Y. D. *Nature Nanotech.*, **2011**, 6, 452-460.

[97] Tesler, A. B.; Chuntonov, L.; Karakouz, T.; Bendikov, T. A.; Haran, G.; Vaskevich, A.; Rubinstein, I. *J. Phys. Chem. C*, **2011**, 115, 24642-24652.

[98] Wojtysiak, S.; Walczyński, M. S.; Kudelski, A. *Vibra. Spectrosc.*, **2011**, 57, 261-269.

[99] Qin, Y.; Ji, X.; Jing, J.; Liu, H.; Wu, H.; Yang, W. *Colloid. Surf. A: Physicochem. Eng. Aspect.*, **2010**, 372, 172-176.

[100] Cao, W. Y.; Jin, R.; Mirkin, C. A. *J. Am. Chem. Soc.*, **2001**, 123, 7961-7962.

[101] Singh, S. P.; Karmakar, B. *Plasmonics*, **2011**, 6, 457-467.

[102] Raschke, G.; Kowarik, S.; Franzl, T.; Sönnichsen, C.; Klar, T. A.; Feldmann, J. *Nano Lett.*, **2003**, 3(7), 935-938.

[103] Anker, J. N.; Hall, W. P.; Lyandres, O.; Shah, N. C.; Zhao, J., Duyne, R. P.V. *Nature Mater.*, **2008**, 7, 442-453.

[104] Marimuthu, A.; Christopher, P.; Linic, S. *J. Phys. Chem. C*, **2012**, 116, 9824-9829.

[105] Schaefer, A.; Ragazzon, D.; Wittstock, A.; Walle, L. E.; Borg, A.; Bäumer, M.; Sandell, A. *J. Phys. Chem. C*, **2012**, 116, 4564-4571.

[106] Barnes, W. L.; Dereux, A.; Ebbesen, T. W. *Nature*, **2003**, 424, 824-830.

[107] Berini, P.; Leon, I. D. *Nature Photon.*, **2012**, 6, 16-24.

[108] Zhu, J.; Li, J.-J.; Yuan, L.; Zhao, J. W. *J. Phys. Chem. C*, **2012**, 116, 11734-11740.

[109] Cialla, D.; März, A.; Böhme, R.; Theil, F.; Weber, K.; Schmitt, M.; Popp, J. *Anal. Bioanal. Chem.*, **2012**, 403, 27-54.

[110] Cobley, C. M.; Skrabalak, S. E.; Campbell, D. J.; Xia, Y. *Plasmonics*, **2009**, 4, 171-179.

[111] Shankar, S. S.; Rizzello, L.; Cinqolani, R.; Rinaldi, R.; Pompa, P. P. *ACS Nano*, **2009**, 3(4), 893-900.

[112] Lee, S. J.; An, H. H.; Han, W. B.; Kim, H.-S.; Yoon, C. S. *Langmuir*, **2012**, 28, 10980-10987.

[113] Li, G.; Song, X.; Sun, Z.; Yang, S.; Ding, B.; Yang, S.; Yang, Z.; Wang, F. *Solid State Sci.*, **2011**, 13, 1379-1384.

[114] Ghosh, S. K.; Rahman, D. S.; Ali, A. L.; Kalita, A. *Plasmonics*, **2013**, 8, 1457-1468.

[115] Sun, H.; Yu, M.; Wang, G.; Sun, X.; Lian, J. *J. Phys. Chem. C*, **2012**, 116, 9000-9008.

[116] Jang, G. G.; Blake, P.; Roper, D. K. *Langmuir*, **2013**, 29, 5476-5486.

[117] Shan, X.; Patel, U.; Wang, S.; Iglesias, R.; Tao, N. *Science*, **2010**, 327, 1363-1366.

[118] López-Tocón, I.; Otero, J. C.; Arenas, J. F.; Garcia-Ramos, J. V.; Sanchez-Cortes, S. *Anal. Chem.*, **2011**, 83, 2518-2525.

[119] Fang, J.; Lebedkin, S.; Yang, S.; Hahn, H. *Chem. Commun.*, **2011**, 47, 5157-5159.

Chapter 2

Experimental

2.1 Preparation of substrates

Plain microscopic glass slides (25×75×1.00 mm) were sliced with a diamond scribe into dimensions of approximately 25×25 mm (1×1 inch). Afterwards, they were immersed in three solvents: ethanol, 0.1M acetic acid and ultrapure water (18.2 MΩ•cm, Barnstead). Then, they were dried with an air gun. Silicon wafers and acetate sheets were exposed to same washing treatment.

2.2 Metal evaporation

The deposition was done with a home built thermal metal evaporator equipped with a vacuum chamber and an inbuilt Inficon XTM/2 JC Controls Deposition Monitor. The thickness of the films was measured at the time of evaporation with an in built Quartz Crystal Microbalance (QCM).

Deposition of Ag and Cr on a glass slide

Silver (Ag) and chromium (Cr) wires were placed on separate tungsten boats. The deposition was done at a chamber pressure of 8.3×10^{-3} torr. Chromium was deposited on the glass slide at rates of 0.5-1.6 Å/s. Its QCM thickness was measured as 34.1 nm. Then,

silver was deposited on top of the chromium at rates of 0.3-0.7 Å/s. Its QCM thickness was measured as 21.4 nm. The sum of the bilayer thickness was 55.5 nm.

Au/Ag thin bilayer on a silicon wafer

Gold (Au) wire was wound across the tungsten coil whereas Ag wire was placed on a boat. The chamber pressure was reduced to 3.4×10^{-4} torr. Then, Ag was deposited on the wafer at rates of 0.8-1.2 Å/s. Its QCM thickness was measured as 230.7 nm. Then, Au was deposited on top of the Ag. The QCM thickness of this layer was unavailable, but calculations from the weight of loaded material gave an approximate thickness of 3.2 nm. Therefore, the thickness of the bilayer film is assumed to be 233.9 nm. Gold was deposited on the thick silver layer to minimize possible oxidation.[1] The Au layers were kept quite thin to advance our goal of a low-cost sensor, while other metal thicknesses were varied. Though SERS studies have been carried out on different materials,[2] the use of metallic thin films on silicon substrates have been very rare.

Au/Ag thick bilayer on a silicon wafer

Au and Ag wires were placed on tungsten coil and boat, respectively. The chamber pressure was reduced to 3.5×10^{-4} torr. Ag was deposited on the wafer at rates of 0.3-2.8 Å/s. Its QCM thickness was measured as 387.4 nm. Then, Au was deposited on top of the Ag at rates of 0.4-0.8 Å/s. Its QCM thickness was measured as 8.2 nm. The sum of the bilayer thickness was 395.6 nm.

Au/Ag mixed layer on a silicon wafer

Au and Ag wires were placed on tungsten coil and boat, respectively. The chamber pressure was reduced to 3.8×10^{-4} torr. The deposition of Au and Ag was done simultaneously with rates of 0.6-1.9 Å/s. Total QCM thickness of the mixed film was 453.8 nm.

Au/Cu bilayer on a silicon wafer

Au wires and copper (Cu) nodules were placed on a tungsten coil and a molybdenum boat, respectively. The chamber pressure was reduced to 2.3×10^{-4} torr. Cu was deposited on the wafer at rates of 0.4-0.5 Å/s. Its QCM thickness was measured as 7.1 nm. Then, Au was deposited on top of the Cu at rates of 0.9-1.7 Å/s. Its QCM thickness was measured as 8.8 nm. The sum of bilayer thickness was 15.9 nm.

Ag deposition on an acetate sheet

The chamber pressure was reduced to 3.3×10^{-4} torr. Ag was deposited on the sheet at rates of 1.2-3.7 Å/s. Its QCM thickness was measured as 260.1 nm.

Cu on an acetate sheet

The chamber pressure was reduced to 3.4×10^{-4} torr. Cu was deposited on the sheet at a maximum deposition rate of 10.3 Å/s. Its QCM thickness was measured as 153.2 nm.

Au/Ag on an acetate sheet

Ag was deposited on the sheet. Its QCM thickness was measured as 260.1 nm. Then, Au was deposited on top of the Ag layer. Its QCM thickness was measured as 6.8 nm. The sum of the bilayer thickness was 266.9 nm.

Au/Cu on an acetate sheet

Cu was deposited on the sheet at rates of 1.2-3.6 Å/s during a chamber pressure of 3.5×10^{-4} torr. Its QCM thickness was measured as 60.7 nm. Then, Au was deposited on top of the Cu at rates of 0.3-0.5 Å/s during a chamber pressure of 3.9×10^{-4} torr. Its QCM thickness was measured as 6.8 nm. The sum of the bilayer thickness was 67.5 nm.

Cu/Ag on an acetate sheet

Ag was deposited on the sheet. Its QCM thickness was measured as 260.1 nm. Then, Cu was deposited on top of the Ag layer. Its QCM thickness was measured as 152.7 nm. The sum of the bilayer thickness was 412.8 nm.

2.3 Annealing of substrates

The samples (except acetate substrates) were annealed at 250, 300, 350, and 400ºC for 2 hours. The furnace (Thermolyne F114300) operated at ramping and cooling rates of 100ºC/h.

2.4 AFM study

The topography of the substrates was measured by a contact mode Atomic Force Microscope (AFM) (MFP-3D Asylum Research) with silicon cantilever (CSC37/Cr/Au, MikroMasch) that had force constants from 0.1 to 0.4 N/m. The images were taken at a scan rate of 0.75 Hz with line measurements of 512 points. Igor Pro 6.31 software was used to acquire sample images and analyze the data, including calculation of root-mean square (RMS) roughness.

2.5 Phenanthrene treatment

2.5.1 Preparation of stock solutions

Solid phenanthrene (molar mass 178.23 g/mol, 98% pure) was obtained from Sigma-Aldrich. To prepare a 1.0 ppm aqueous solution of this compound, 1 mg solid phenanthrene was dissolved in 1L of ultrapure water. In order to dissolve all of the phenanthrene, the solution was sonicated for 60 min and allowed to stand for a day. For a 1.6 ppm solution of this compound, 1.6 mg of the analyte was dissolved in 1L of ultrapure water. It was treated in the same manner as the 1.0 ppm solution. The maximum solubility of phenanthrene in water at 25ºC is 1.6 mg/L, therefore, we kept the highest concentration as 1.6 ppm. The quantity of phenanthrene required in preparing solutions of less than 1.0 ppm requires series dilution, so we kept the lowest concentration as 1.0 ppm.

2.5.2 Substrate exposure to phenanthrene solutions

Metal-glass and metal-silicon substrates were immersed in the 1.6 ppm solution of phenanthrene for 30 min. The substrates were rinsed with ultrapure water to remove unbound phenanthrene. The Raman spectral measurement was done after drying the sample at room temperature.

Metal-acetate substrates were treated with the 1.0 ppm solution first. After subsequent water rinsing, the Raman measurement was completed. Before the substrates were exposed to the 1.6 ppm solution, they were rinsed with copious amounts of ethanol. Water rinsing was done as before.

2.6 Raman spectral measurement

Raman spectra were recorded with a bench top spectrometer (Renishaw inVia, UK) that had a laser beam of 830 nm and 1200 lines/mm grating. The laser was kept low at 10% power to avoid possible sample damage and the integration time was fixed at 10 s. The light was focused using a microscope objective of 50× (Leica microscope). Prior to the sample run, the instrument was calibrated with silicon at 520.5 cm^{-1}. The spectra were measured from 100 to 3200 cm^{-1} using extended scanning mode. The spectral analysis was performed with Renishaw WiRE 3.4 and Igor Pro 6.31 software.

2.7 SEM and EDX studies

FEI Quanta 650 FEG Scanning Electron Microscope (SEM) equipped with a Bruker XFLASH 5030 SDD X-ray detector (Energy Dispersive X-ray, EDX) characterized the morphology of the films and the elemental composition.

Bibliography

[1] Fu, C. Y.; Kho, K. W.; Dinish, U. S.; Koh, Z. Y.; Malini, O. *J. Raman Spectrosc.*, **2012**, 43, 977-985.

[2] Liu, J.-W.; Wang, J.-L.; Huang, W.-R.; Yu, L.; Ren, X.-F.; Wen, W.-C.; Yu, S.-H. *Sci. Reports*, **2012**, 2, 987 (1-7).

Chapter 3

Substrate characterization

3.1 Ag/Cr/glass substrate

AFM analysis

The RMS roughness of the Ag/Cr bilayer was measured by AFM. For each sample, an average value of three different measurements was reported as the surface roughness. The preannealed sample possessed a roughness of 20.81 nm whereas the sample annealed at 400ºC had the highest roughness (67.71 nm). Roughness for this and other samples on glass and silicon are summarized in Table 3.1.1.

Table 3.1.1: Roughness of different substrates (nm); each value is an average of three measurements, with the standard deviation within parentheses.

Annealing temperature	Ag/Cr glass	Au/Ag mixed	Au/Ag thin	Au/Ag thick	Au/Cu
Preannealed	20.81 (0.77)	5.40 (0.16)	2.74 (0.63)	1.52 (0.00)	0.33 (0.05)
250ºC	20.48 (2.10)	7.62 (2.08)	3.24 (0.33)	6.98 (0.32)	1.29 (0.09)
300ºC	53.04 (8.74)	250.16 (23.33)	27.40 (2.23)	40.59 (3.21)	6.78 (0.08)
350ºC	52.67 (2.43)	265.33 (4.57)	39.93 (1.63)	62.24 (0.29)	17.75 (0.19)
400ºC	67.71 (1.44)	223.81 (4.43)	121.34 (2.39)	117.47 (0.85)	16.44 (0.08)

The annealing process changes surface morphology by increasing the number of clusters and bumps on the surface (Figure 3.1.1). This leads to an increase in surface roughness.

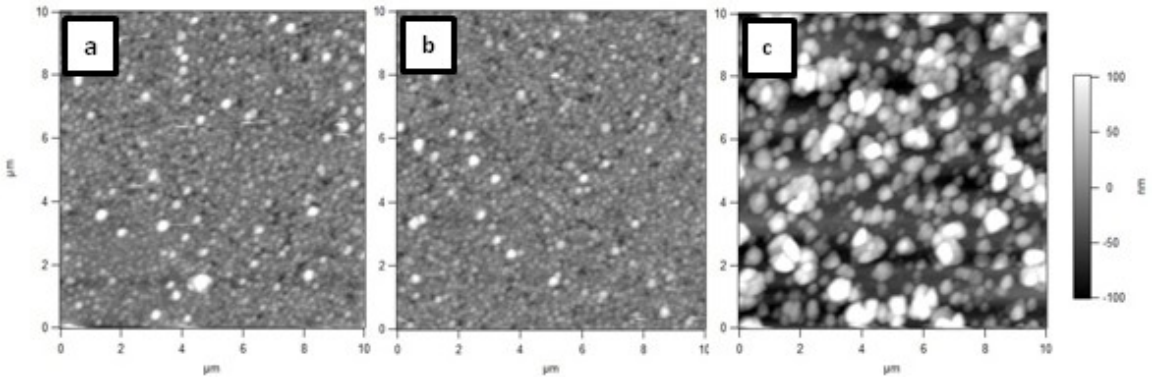

Figure 3.1.1: AFM images of the Ag/Cr bilayer deposited on a glass surface: (a) pre-annealed, (b) annealed at 250ºC, and (b) annealed at 400ºC. The figures show how the annealing process caused a change in surface morphology as well as surface roughness.

SEM and EDX studies

The SEM images of the preannealed Ag/Cr substrate show high levels of Cr, but low levels of Ag.

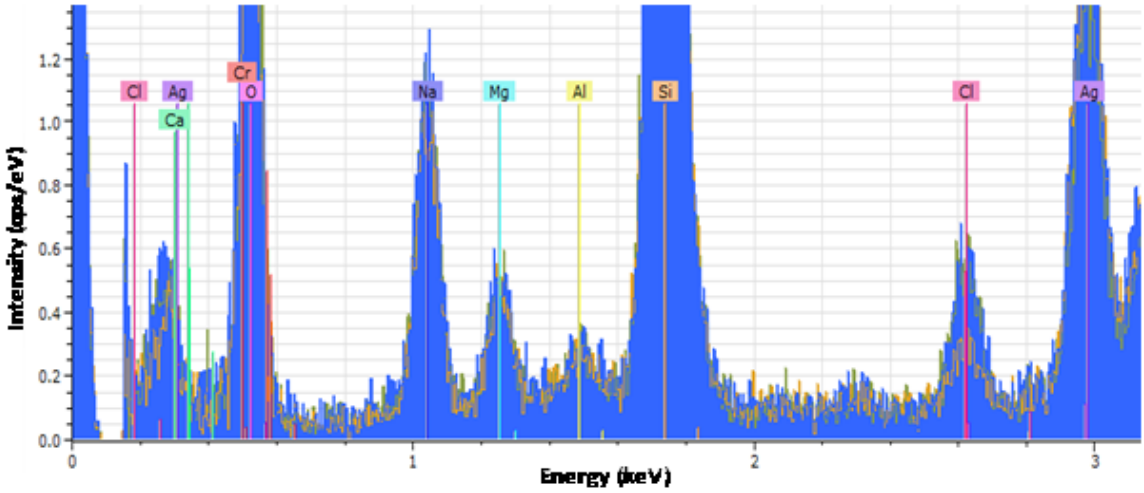

Figure 3.1.2: EDX spectrum for the Ag/Cr bilayer sample annealed at 300ºC. An abundance of silver was observed at 2.94 keV.

The sample annealed at 300ºC contained high levels of Ag (Figure 3.1.2). The sample annealed at 350ºC contained a lower amount of Ag. However, no signal from Cr is visible. This indicates that there was a continuous layer of Ag over the Cr layer at this temperature.

The Ag/Cr substrates deposited on a glass and annealed at lower temperatures contain a continuous Cr layer and Ag clusters on top of the Cr layer. The SEM and AFM images of the Ag/Cr bilayer films display an irregular distribution of surface clusters. This means that there is no uniformity in the surface roughness.

3.2 Au/Ag thin bilayer

AFM analysis

The Au/Ag thin bilayer deposited on a silicon wafer shows an increasing surface roughness with increasing annealing temperature (Figure 3.2.1). The lowest roughness (2.74 nm) was observed in the preannealed sample and the highest roughness (121.34 nm) was observed in the sample annealed at 400ºC.

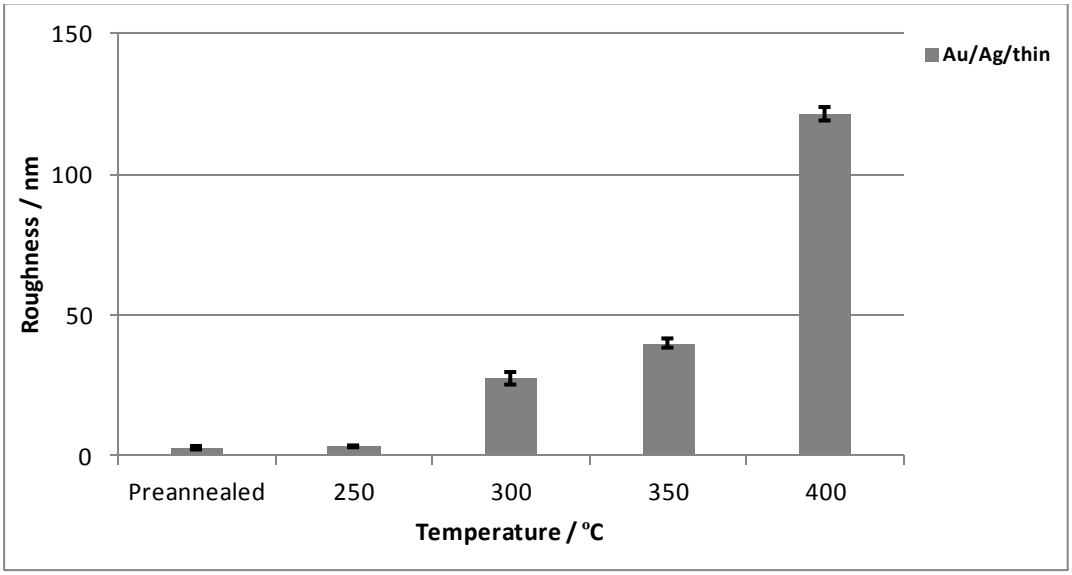

Figure 3.2.1: Change in surface roughness with a change in annealing temperature for the Au/Ag thin bilayer substrates prepared on a silicon wafer. Each measurement is made in triplicate. The corresponding data is shown in Table 3.1.1.

SEM and EDX studies

The EDX spectra for all samples (preannealed, annealed at 250, 300, 350, and 400ºC) look the same. According to the SEM results, the metals clustered. The distance between

clusters are in the order of 0.5 μm. Although the beam diameter is on the order of 10 nm, the electron interaction volume inside the sample is above 1 μm. Therefore, it is not possible to discern if there were any traces of metals still left between the clusters. All spectra contained traces of Mg and Al. These metals could have come from the deposition chamber or from the electron scattering process.

3.3 Au/Ag thick bilayer

AFM analysis

The variation in surface roughness in the thick bilayer substrates is similar to the variation observed in the thin bilayer. The preannealed sample had the lowest roughness (1.52 nm) whereas the sample annealed at 400ºC had the highest roughness (117.47 nm).

SEM and EDX studies

The SEM images of the Au/Ag thick bilayer samples show that the bilayer forms a cluster array with increased annealing. The EDX data for these bilayer samples resembles the EDX data for the thin bilayer.

3.4 Au/Ag mixed film

AFM analysis

The surface roughness for the Au/Ag mixed film increases up to an annealing temperature of 350ºC and subsequently declines at an annealing temperature of 400ºC (Figure 3.4.1).

The AFM images (Figure 3.4.2) show shrinkage of cluster size from 350ºC to 400ºC. This may cause a decrease in surface roughness.

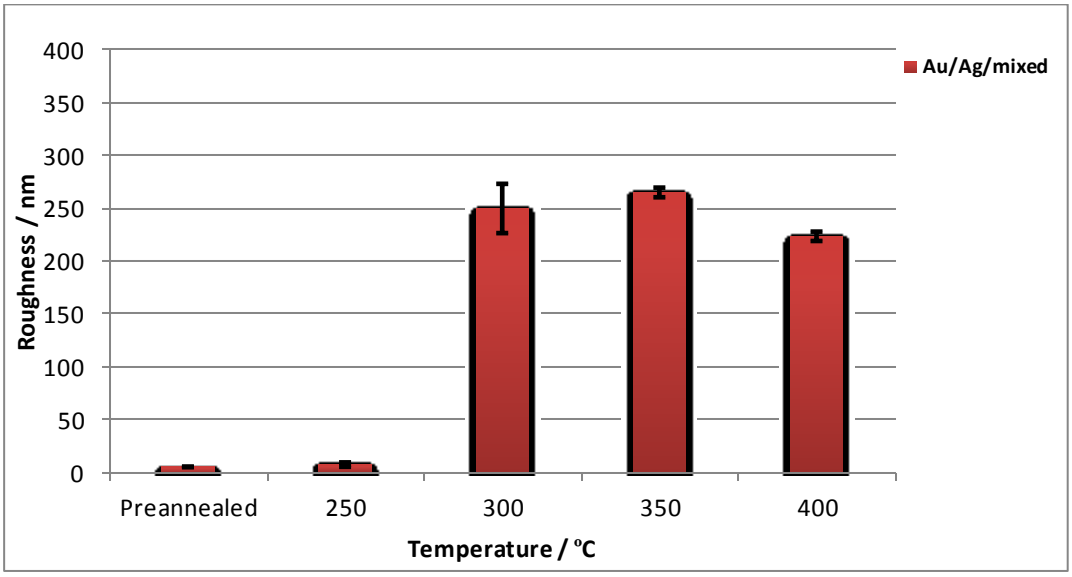

Figure 3.4.1: The change in surface roughness with change in annealing temperature for the Au/Ag mixed film. Each measurement is made in triplicate. The corresponding data is shown in Table 3.1.1.

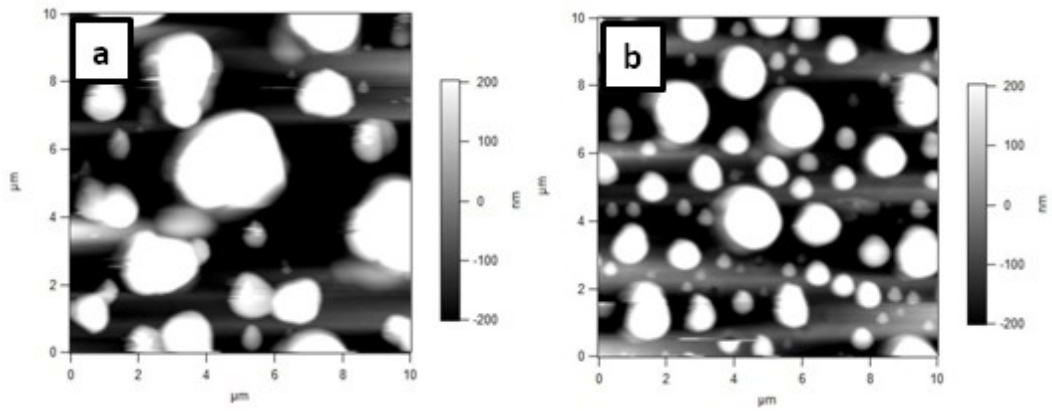

Figure 3.4.2: AFM images of the Au/Ag mixed film deposited on a silicon wafer: (a) annealed at 350ºC and (b) annealed at 400ºC. Annealing from 350ºC to 400ºC reduced the grain size. This may have caused a decrease in surface roughness.

SEM and EDX studies

According to the SEM images, samples annealed at 350ºC and 400ºC form discrete clusters ranging in size from 100 nm to 2 μm. The surface fraction of these clusters is reduced significantly in comparison to the samples annealed at 250ºC and 300ºC. There is a peak in the EDX spectra of the samples annealed at 350ºC and 400ºC at approximately 3.48 keV. This peak corresponds to Si. Therefore, the electron beam interaction volume is larger than the size of the clusters.

3.5 Au/Cu bilayer

AFM analysis

The surface roughness of the Au/Cu bilayer films increases as the temperature increases, except at 350ºC. A relatively small surface roughness for the Au/Cu thin films compared to the Au/Ag substrates is attributed to the formation of smaller clusters (Figure 3.5.1). This could be due, in part, to the fact that the Au/Cu bilayer is thinner to begin with, however, quite high roughness can be achieved from dewetting of even thin films. The Au grain size and separation (to enhance the SERS response) can be tuned through varying composition of the bilayer as well as its thickness.

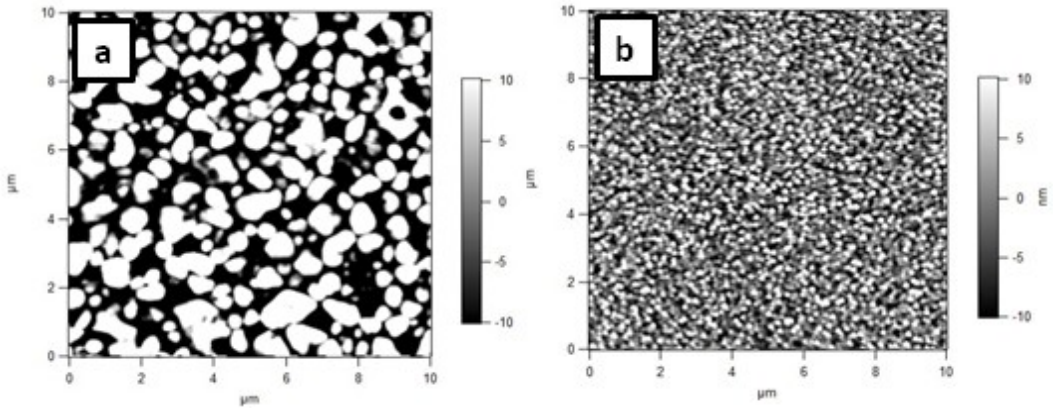

Figure 3.5.1: AFM images of (a) the Au/Ag thick bilayer and (b) the Au/Cu bilayer. Both were deposited on a silicon wafer and annealed at 300ºC. The images show a difference in surface grain size. The Au/Ag thick bilayer (with a relatively large grain size) has a surface roughness of 40.59 nm whereas the Au/Cu bilayer (with smaller grains) has a surface roughness of only 6.78 nm.

SEM and EDX studies

The EDX spectra reveal that all of the spectra have a peak at 3.48 keV that is caused by Si. The Au peak at 0.247 keV in the sample annealed at 350ºC has a higher intensity in comparison to the same peak in other samples (preannealed and annealed).

Unlike the Au/Ag bilayer films, there is discrete clustering at increased annealing temperatures in the Au/Cu samples (Figure 3.5.2).

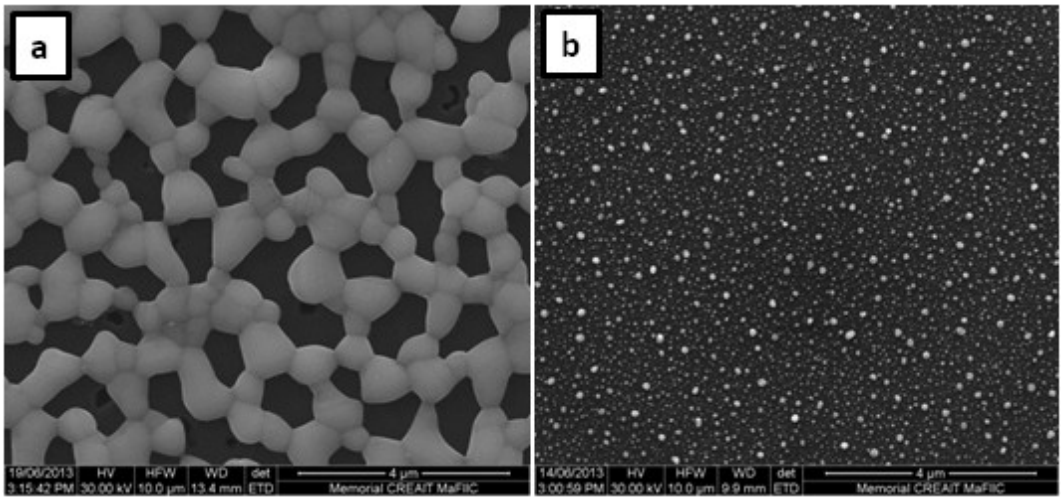

Figure 3.5.2: SEM images: (a) Au/Ag thin bilayer and (b) Au/Cu bilayer. Both were deposited on a silicon wafer and annealed at 400ºC. The Au/Ag bilayer formed continuous beads at elevated annealing temperatures, but the Au/Cu bilayer formed discrete and isolated clusters.

3.6 Acetate substrates

Metal-acetate substrates are opaque in nature, as seen in the optical photographs in Figure 3.6.1. As outlined in the next chapter, these substrates presented problems for use in SERS-based detection; therefore, further microscopic studies were not carried out.

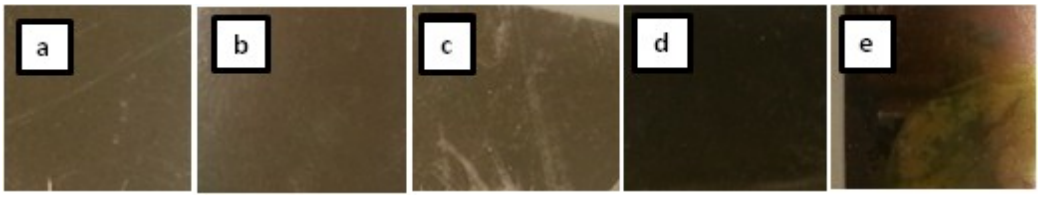

Figure 3.6.1: Metal-acetate substrates: (a) Ag/acetate, (b) Cu/acetate, (c) Au/Ag/acetate, (d) Au/Cu/acetate, and (e) Cu/Ag/acetate. In (c) and (d), the top layer was Au whereas the top layer was Cu in (e).

Chapter 4

SERS enhancement studies on the prepared substrates

4.1 Metal-silicon substrates

4.1.1 Au/Ag thin bilayer

The SERS spectrum for the Au/Ag thin bilayer substrate annealed at 300ºC and the Raman spectrum of solid phenanthrene are shown in Figure 4.1.1.1.

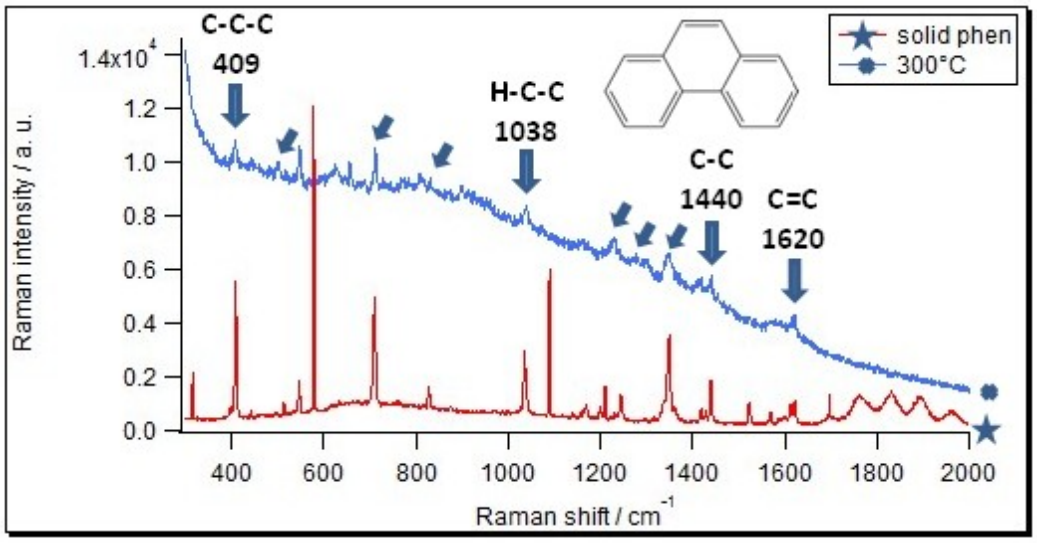

Figure 4.1.1.1: SERS spectrum of phenanthrene on a Au/Ag thin bilayer deposited on a silicon wafer and annealed at 300ºC. The Raman spectrum of solid phenanthrene is shown for an easy comparison. The arrows (vertical and diagonal) indicate the SERS enhancement of phenanthrene; the vertical arrows show the principal vibrational modes.

Results

Substrate annealed at 300ºC: Characteristic phenanthrene peaks were observed at 409, 443, 503, 549, 713, 831, 1038, 1233, 1350, 1416, 1440, 1615, and 1620 cm^{-1}.

Assignment of main peaks: The peak at 409 cm^{-1} was assigned to the C-C-C bending vibrations[1] and the peak at 1038 cm^{-1} was assigned to the H-C-C bending vibrations.[2] The peak at 1440 cm^{-1} was caused by the C-C stretching vibrations of the benzene ring.[1,2] However, an intense Raman peak for silver particles was found at 1441 cm^{-1} as well.[3] The peak at 1620 cm^{-1} is due to the aromatic C=C stretching vibrations.[1] In fact, the peaks that appeared around 410 (C-C-C bending), 1040 (H-C-C bending), 1440 (aromatic C-C

stretching), and 1620 (aromatic C=C stretching) cm^{-1} were assumed as the fundamental vibrational modes of phenanthrene. The Au/Ag thin bilayer annealed at 300ºC exhibited all of these vibrations. Therefore, the SERS spectrum of this sample was placed alongside the Raman signals of solid phenanthrene for an easy comparison. To avoid spectral complexity, the Raman spectrum of the solid phenanthrene was removed in subsequent analyses.

Assignment of other peaks: The peak at 503 cm^{-1} was caused by the skeletal deformation vibrations[4] and the peak at 1231 cm^{-1} was assigned to the presence of C-H in-plane bending vibrations.[4] Moreover, the peaks at 1350 and 1416 cm^{-1} were assigned to the C-C stretching vibrations of the benzene ring.[1,5] Also, aromatic C=C stretching vibrations were observed at 1615 cm^{-1}.[1] The Raman spectrum of solid phenanthrene exhibited a signal at 1242 cm^{-1} that corresponds to H-C-C bending.[1] Therefore, the peak at 1233 cm^{-1} was believed to be caused by the H-C-C bending vibrations of the liquid phenanthrene. The peak at 443 cm^{-1} was probably caused by the presence of AgO particles[6] whereas the peak at 659 cm^{-1} was caused by silver particles.[3] Unassigned peaks were observed at 626, 770, 809, and 900 cm^{-1}.

Preannealed substrate: The preannealed substrate gave characteristic phenanthrene peaks at 409, 491, 616, 710, and 1037 cm^{-1} (Figure 4.1.1.2). The preannealed substrate had the lowest SERS enhancement. The peaks at 409 and 1037 cm^{-1} were assigned to the C-C-C bending and H-C-C bending vibrations, respectively.[1]

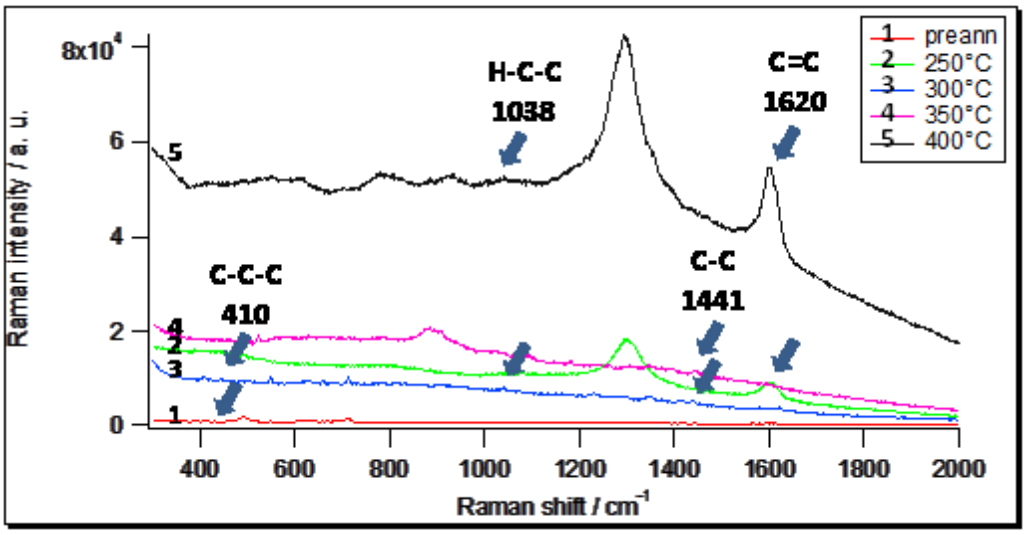

Figure 4.1.1.2: SERS spectra of phenanthrene on a Au/Ag thin bilayer deposited on a silicon wafer. The temperatures indicate annealing of the substrate prior to exposure of phenanthrene. The arrows show the positions of the main phenanthrene peaks.

Substrate annealed at 250°C: Two quite distinct phenanthrene peaks were observed at 1038 and 1602 cm^{-1}. The peak at 1038 cm^{-1} was assigned to the C-C-C bending vibrations[1] and the peak at 1602 cm^{-1} was assigned to aromatic C=C stretching vibration.[7] The peak at 1301 cm^{-1} is not assigned to phenanthrene and may be due to fluorescence.

Substrate annealed at 350°C: Characteristic phenanthrene peaks were found at 716, 1183, and 1445 cm^{-1}. The silicon peak (523 cm^{-1}) for this sample was well pronounced. The signal at 1445 cm^{-1} was assigned to aromatic C-C ring stretching vibrations[1] and the peak at 1095 cm^{-1} was believed to be caused by silver particles.[3] The characterization of the peaks at 885 and 1301 cm^{-1} are unknown.

Substrate annealed at 400ºC: Characteristic phenanthrene peaks occurred at 1048 and 1603 cm^{-1} which were assigned to the H-C-C bending and aromatic C=C stretching vibrations, respectively.[1,7]

Discussion

The results of the aqueous phenanthrene-treated Au/Ag thin bilayer show that the annealing process causes an enhancement of SERS response. However, the sample annealed at 300ºC exhibited the most peaks compared to the other samples. Although the sample annealed at 400ºC gave the highest signal, it was highly influenced by background fluorescence. In terms of a large SERS enhancement and small background fluorescence, the sample annealed at 300ºC are considered to be the best SERS-active material. Therefore, an annealing temperature of 300ºC is considered to be the ideal one at which the best SERS-response could be achieved to detect PAHs using Au/Ag substrates.

There are two shifts in the position of the phenanthrene peaks in the spectra for the Au/Ag thin films. The large signal at 1350 cm^{-1} in the solid analyte, which was assigned to the C-C stretching vibrations,[1] was moved to 1341 (at 300ºC), 1304 (at 350ºC), 1297 (at 250ºC), and 1296 cm^{-1} (at 400ºC) with a corresponding increase in peak intensity. The solid phenanthrene peak at 1624 cm^{-1} was moved to 1622 (at 300ºC), 1602 (at 250ºC), 1595 (at 350ºC), and 1598 cm^{-1} (at 400ºC). These signal movements may be caused due to bonding interactions between the analyte and the metal surface.[7]

The SEM images revealed that the annealing process formed a continuous metal cluster on the surface. The sample annealed at 300ºC gave rise to the development of more compact layers (approximate gaps of 0.2 μm between two clusters), thereby leaving smaller uncovered surface sites. Also, a large SERS enhancement for the sample annealed at 300ºC may have arisen because of a strong plasmonic interaction between closely distributed metal clusters.[8] As the annealing temperature increased from 300ºC to 350ºC, the metal layers became more compact (approximate gaps of 1.0 μm between two clusters). This resulted in even more uncovered silicon surfaces. As a result, the surface site became unavailable for stronger plasmonic interactions. This reduced the SERS intensity at this temperature. The SEM images (Figure 4.1.1.3) show a clear evidence of this phenomenon.

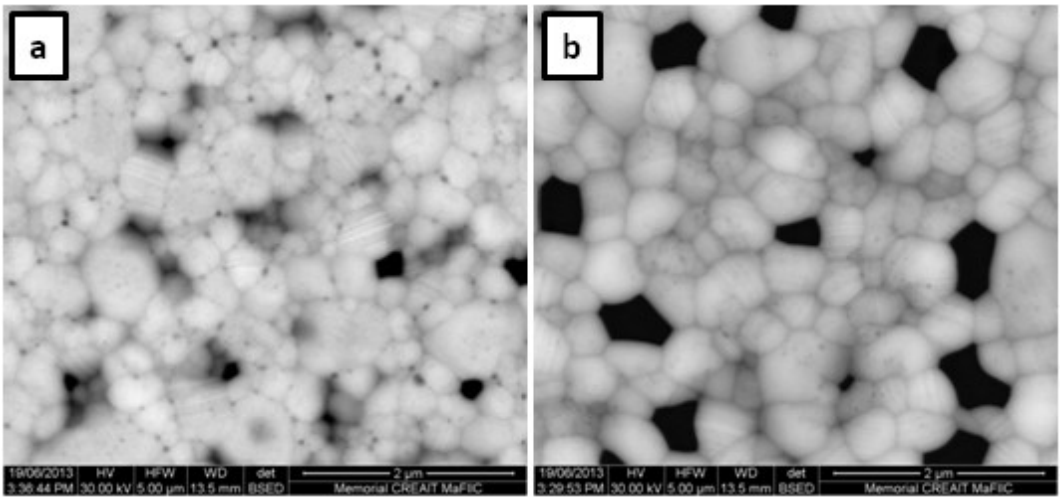

Figure 4.1.1.3: SEM images of the Au/Ag thin bilayer samples: (a) annealed at 300ºC and (b) annealed at 350ºC.

4.1.2 Au/Ag thick bilayer

The SERS spectra for the Au/Ag thick bilayer are shown in Figure 4.1.2.1.

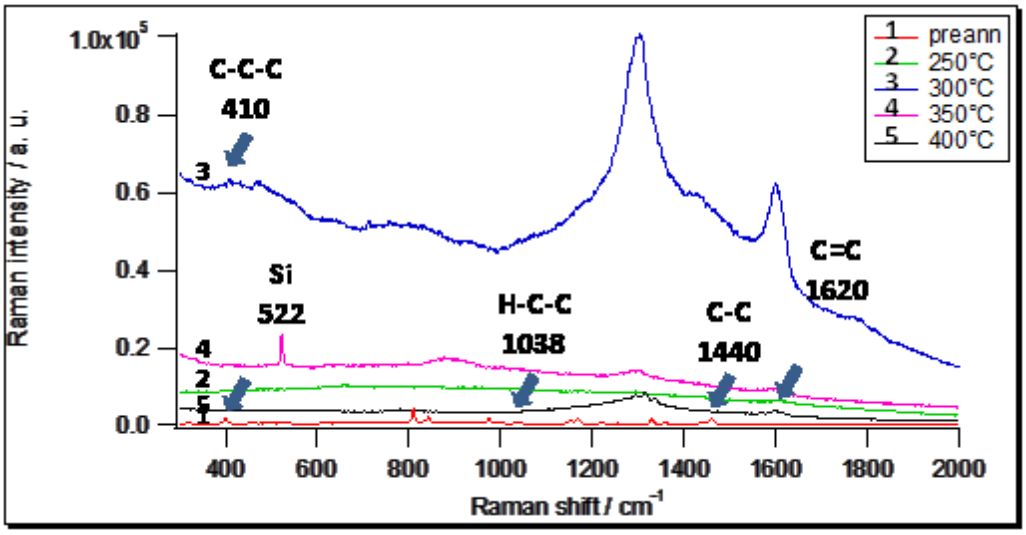

Figure 4.1.2.1: SERS spectra of phenanthrene on a Au/Ag thick bilayer deposited on a silicon wafer. The arrows illustrate the main phenanthrene peaks.

Results

Preannealed substrate: It showed phenanthrene signals at 406, 710, 1001, 1037, 1169, 1364, and 1440 cm^{-1}. The peaks at 406 and 1037 cm^{-1} were assigned to the C-C-C bending and H-C-C bending vibrations, respectively.[1] The signal at 1364 cm^{-1} was due to C-C vibrations in the aromatic ring.[5] Also, the peak at 1440 cm^{-1} was caused by the C-C stretching vibrations of aromatic ring.[1] The signal at 1001 cm^{-1} was believed to be caused by the combined effects of C-C stretching and C-H rocking vibrations.[9] Peaks with unknown characterizations were observed at 458, 530, 811, 843, 902, 943, 974, 1154, 1222, 1256, 1332, and 1461 cm^{-1}.

Substrate annealed at 250ºC: Two small bumps were observed at 1331 and 1624 cm^{-1}. The peak at 1624 cm^{-1} was due to C=C vibrations of aromatic ring.[1]

Substrate annealed at 300ºC: A phenanthrene peak was observed at 409 cm^{-1} and a small bump was observed at 471 cm^{-1}. The peak at 409 cm^{-1} was assigned to the C-C-C bending vibrations.[1] Two intense fluorescence peaks were observed at 784 and 1296 cm^{-1}.

Substrate annealed at 350ºC: An intense silicon peak was observed at 522 cm^{-1} and a small phenanthrene signal was found at 713 cm^{-1}. The bump at 1593 cm^{-1} was assigned to stretching vibrations in the aromatic ring.[10] Two bumps with unknown characterizations were found at around 880 and 1302 cm^{-1}.

Substrate annealed at 400ºC: Phenanthrene peaks were found at 1296, 1317, 1339, and 1599 cm^{-1}. The peak at 1599 cm^{-1} was assigned to the aromatic C=C stretching vibratiions.[7] The peak at 1339 cm^{-1} was assigned to the H-C-C bending vibrations.[2]

Discussion

In the Au/Ag thick bilayer, the SERS intensity of the preannealed sample was comparable to that of solid phenanthrene. This spectral feature was observed in thin bilayer substrates as well. Also, like the thin bilayer, there were shifts in the position of two phenanthrene peaks. The peak that appeared at 1351 cm^{-1} in solid phenanthrene, assigned to the C-C stretching vibrations,[1] was moved to 1331 (at 250ºC), 1317 (at 400ºC), 1302 (at 300ºC), and 1300 cm^{-1} (at 350 ºC). The characteristic phenanthrene signal at 1615 cm^{-1} was moved to 1624 (at 250ºC), 1603 (at 400ºC), 1596 (at 350ºC), and 1598 cm^{-1} (at 300ºC). These shifts may have taken place because of the bonding interactions between phenanthrene and the surface of the bilayer.[7] As with the thin bilayer substrates, the peak shifted to a lower wavenumber with increased annealing. The sample annealed at 300ºC was heavily affected by fluorescence compared to the other samples. In contrast, the thin bilayer substrate that was most affected by fluorescence was the sample annealed at 400ºC.

The SEM images showed that samples clustered at elevated temperatures (Figure 4.1.2.2). An intense silicon peak at 523 cm^{-1} for the sample annealed at 350ºC revealed that, as the sample clustered, there was a wide distribution of particles that resulted in more uncovered surface sites.

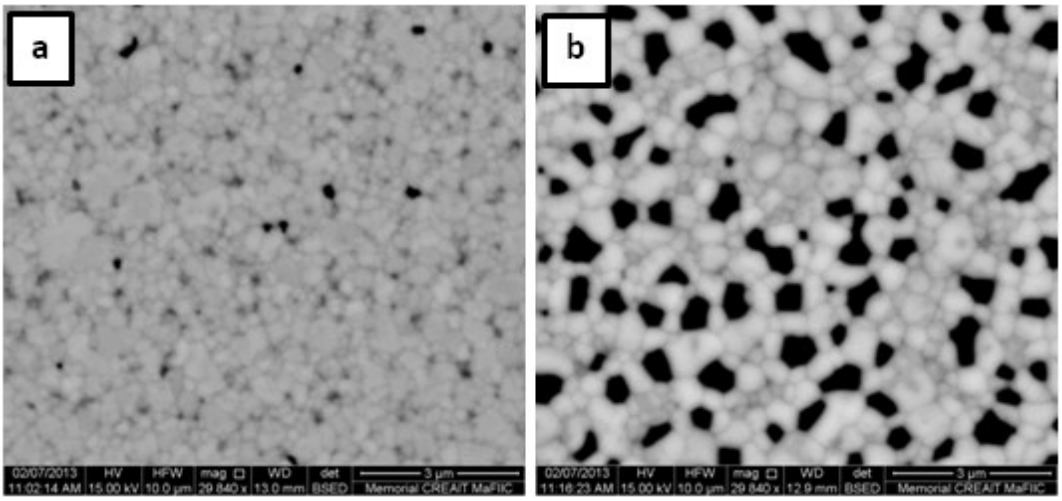

Figure 4.1.2.2: The SEM images of the Au/Ag thick bilayer samples: (a) annealed at 250ºC and (b) annealed at 350ºC. The images show that (a) possessed an average distance of 0.3 µm between clusters, but (b) possessed an average distance of 1.2 µm between clusters. Annealing made the uncovered surface even more pronounced, thereby leaving insufficient beads of clusters for surface plasmon resonance. This may have caused the weak SERS response for substrates annealed at 350ºC.

Metal thickness and SERS enhancement

In the thin substrates, the thickness of the top (Au) layer was 3.18 nm and the thickness of the bottom (Ag) layer was 230.7 nm. The thickness of this bilayer was 233.9 nm. In the thick substrates, the thickness of the top (Au) layer was 8.2 nm and the thickness of the bottom (Ag) layer was 387.4 nm. The thickness of this bilayer was 395.6 nm. As a result, the thick bilayer contained more gold and silver. The results reveal that the thin bilayer exhibited a greater SERS enhancement than the thick bilayer. Fu *et al.*[11] observed that excessive coating by silver can decrease the SERS intensity. An arbitrary metal thickness

is undesirable to elicit a strong SERS response. A big SERS enhancement is found when the frequency of the incident radiation matches the surface plamonic resonance frequency of the metal particles.[12,13] If Raman excitation wavelength of 785 nm is used, a thin silver layer of 15 to 25 nm is sufficient to generate enough plasmonic signals.[11] Generally, strong plasmonic resonance arises if the metal thickness is below 10 nm.[11] In this study, the SERS spectra were collected with an 830 nm excitation wavelength. There was good agreement with the results from this study and the experimental set-up followed by the previous research group[11] to get a big SERS response.

The SEM images reveal that the thick bilayer contained large pinholes with approximate sizes ranging from 1.0 to 2.0 μm. This happened because the thick layer gave rise to the formation of bigger clusters by combining small particles together.[11] The small surface area that was covered with metal beads in the thick film did not allow as many Raman signals to be produced from the phenanthrene solution as expected. As a result, the thick layer provided a weaker SERS response than the thinner one. This result illustrated the dependency of a good SERS enhancement on metal thickness. Furthermore, experimental evidence shows that the intensity of SERS signals is greatly reduced if the substrate contains a top gold layer with a thickness higher than 200 nm.[11]

4.1.3 Au/Ag mixed film

The SERS spectra for the Au/Ag mixed substrates are shown in Figure 4.1.3.1.

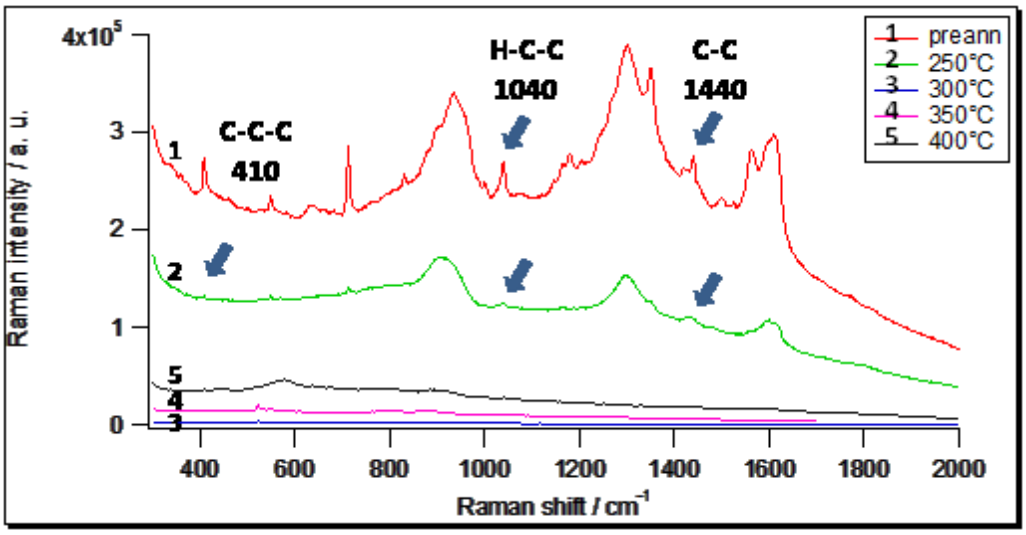

Figure 4.1.3.1: SERS spectra of phenanthrene on a Au/Ag mixed layer deposited on a silicon wafer. The arrows show the positions of the main phenanthrene peaks.

Results

Preannealed substrate: Major phenanthrene peaks were observed at 550, 712, 833, 1040, 1351, 1441, and 1563 cm^{-1}. The peak at 550 cm^{-1} was assigned to the C-C-C bending vibrations.[1] The peaks at 1040 and 1351cm^{-1} were assigned to the H-C-C bending and C-C stretching vibrations, respectively.[1,5] The peak at 1441 cm^{-1} was due to aromatic C-C ring vibrations.[1] However, an intense Raman peak corresponding to silver particles was observed at 1441 cm^{-1} as well.[3] The peak at 1563 cm^{-1} was believed to be caused by the C-C ring vibrations.[1] Peaks with an unknown characterization appeared at 934, 1182, 1301, 1501, and 1512 cm^{-1}.

Substrate annealed at 250ºC: Characteristic phenanthrene peaks occurred at 412, 551, 714, 1040, and 1441 cm^{-1}. The signals found at 412 and 551 cm^{-1} were assigned to the C-

C-C bending vibrations[1] whereas the peak at 1040 cm^{-1} was assigned to the H-C-C bending vibrations.[1] The strong peak at 1441 cm^{-1} was due to the C-C stretching vibrations of the aromatic ring.[1] Peaks with an unknown characterization appeared at 1166 and 1298 cm^{-1}.

Substrate annealed at 300ºC: The peak at 521cm^{-1} was the characteristic peak of silicon.

Substrate annealed at 350ºC: Phenanthrene signals appeared at 711 and 809 cm^{-1}. The peak at 522 cm^{-1}corresponds to silicon.

Substrate annealed at 400ºC: Characteristic phenanthrene peaks were observed at 405, 577, 714, 805, 1001, and 1201 cm^{-1}. The intense peak at 431 cm^{-1} was assigned to the presence of silver oxides (AgO).[6] The peaks at 405 and 1200 cm^{-1} were assigned to the C-C-C bending and H-C-C bending vibrations, respectively.[1] The peak at 805 cm^{-1} was assigned to the C-H out-of-plane bending vibrations.[14] The peak at 1001 cm^{-1} was believed to be caused by the combined effects of C-C stretching and C-H rocking vibrations.[9] At this temperature, the silicon peak (523 cm^{-1}) was much more pronounced.

Discussion

For the Au/Ag mixed films, a large SERS enhancement was found using the preannealed sample, but it was highly influenced by background fluorescence. This finding is in contrast to the findings from the two Au/Ag bilayer films. In those cases, the preannealed samples were influenced the least by fluorescence. Like the bilayer substrates, there were shifts in the position of phenanthrene peaks. The signal at 578 cm^{-1} in solid phenanthrene was moved to 549 (preannealed), 551 (at 250ºC), and 549 cm^{-1} (at 400ºC). The peak at

712 cm^{-1} was moved to 711 (preannealed), 714 (250ºC), and 715 cm^{-1} (400ºC). Unlike the Au/Ag bilayer substrates, the mixed films exhibited a band shift towards higher wavenumbers with increased annealing. These signal displacements were attributed to the formation of bonding interactions between phenanthrene and the metal surface.[7]

The SEM images reveal that, at a relatively low annealing temperature (300ºC), the surface of the film was mostly covered by continuous metal layers. Small crevices that were only 0.5 µm in diameter were visible. As annealing increased up to 400ºC, discrete clusters with approximate sizes of 0.5 to 1.5 µm were produced (Figure 4.1.3.2). The wider distribution of metal clusters at a higher temperature such as 400ºC could form poor plasmonic hot spots that would render the substrate a weak material for enhancing Raman signals with SERS. However, at higher annealing temperature, the cluster formed a more spherical shape. This observation was confirmed by the UV-vis absorption spectra of the mixed film. According to Mie theory, spherical particles exhibit a single surface plasmonic resonance band whereas anisotropic particles exhibit more than one absorption peak in the UV-vis spectra.[3] The plasmonic resonance band for the spherical silver particles was found at around 400 nm.[15] The UV-vis spectra for the mixed layers that were preannealed and annealed at 250ºC showed principal absorption peaks at 417, 436, 470, and 523 nm. The absorption maximum gradually disappeared as the particles became more spherical in shape at higher temperatures (350ºC and 400ºC). Also, a small absorption band was observed at 499 nm at these higher temperatures.

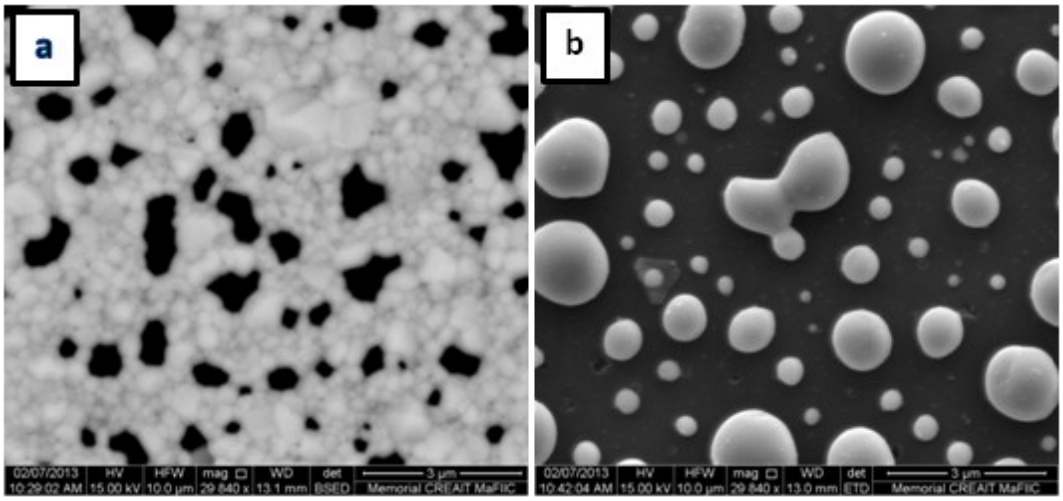

Figure 4.1.3.2: SEM images display the effect of annealing on shape of, size of, and distance between clusters in the Au/Ag mixed film deposited on a Si wafer. Image (a) shows that the sample annealed at 300ºC formed interlinked beads (with an approximate gap of 0.5 μm) whereas (b) shows the formation of spherical clusters at 400ºC. The latter caused an increase in the distance between two clusters (0.5 to 1.5 μm) that could be responsible for the poor SERS enhancement.

SERS enhancement on Au/Ag bilayers and mixed layer

The thickness of the mixed layer was 453.8 nm whereas the thin bilayer had a thickness of 233.9 nm and the thick bilayer had a thickness of 395.6 nm. Therefore, the mixed layer contained almost the same amount of gold and silver as the thick bilayer. The SERS signals of these films revealed that the preannealed samples of the thick bilayer and mixed film exhibited a higher SERS enhancement compared to other samples. The SEM images showed that the annealing process allowed the bilayers to form continuous beads that were evenly distributed on the silicon surface. However, it showed that the mixed

films formed discrete clusters at a higher annealing temperature (400ºC). These clusters had spherical shapes and a large interparticle distance. The much wider distribution of particles in the mixed film at an elevated annealing temperature caused the mixed film to exhibit even weaker SERS responses than the bilayers. Therefore, the mixed films are less promising in devising a molecular sensor.

4.1.4 Au/Cu bilayer

The SERS spectra of the Au/Cu bilayer substrates are shown in Figure 4.1.4.1.

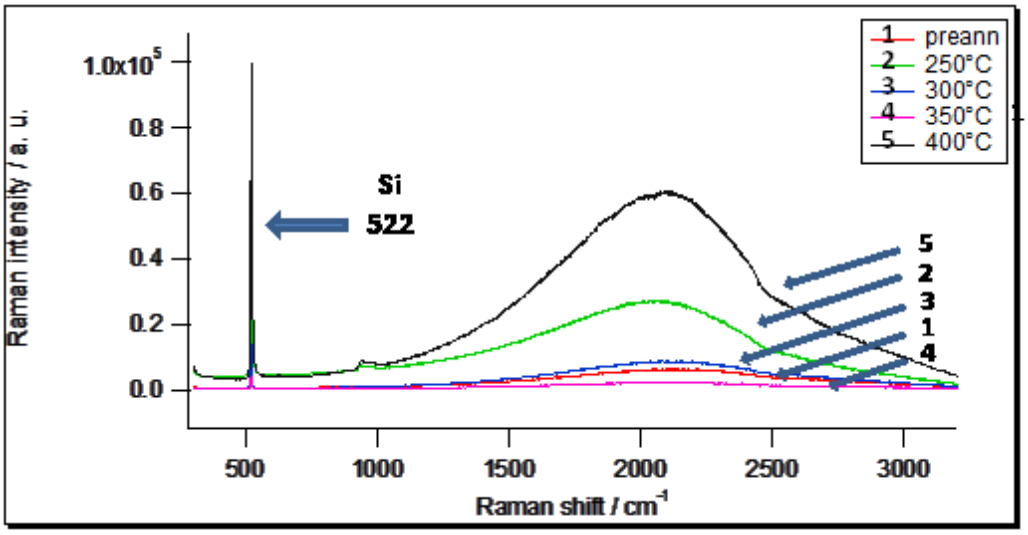

Figure 4.1.4.1: SERS spectra of phenanthrene on a Au/Cu bilayer deposited on a silicon wafer.

Results

The Au/Cu substrates exhibited a broad peak at around 2100 cm^{-1}. The sample with the highest shoulder intensity was the sample annealed at 400ºC. The silicon peak (522 cm^{-1}) was the most intense in all samples.

Discussion

Annealing of the Au/Cu bilayer samples formed isolated clusters with irregular size and shape. Aggregated metal particles show a larger SERS enhancement than isolated ones.[8] In the case of gold films, it was observed that strong plasmonic responses are usually found with interparticle gaps of 2 to 27 nm.[16,17] However, the SEM images revealed that the Au/Cu bilayer that was annealed at 350ºC possessed interparticle gaps that were between 100 and 200 nm. This was the biggest particle separation found in all of the bilayer samples (Figure 4.1.4.2). The large interparticle gap made the silicon surface even more exposed than usual. Therefore, sufficient plasmonic hot spots were not able to form and the resulting weak plasmonic resonance may have caused a decrease in intensity of the SERS signals.[18] The intense Raman signal at 522 cm^{-1} was evidence of a barren silicon surface. This was confirmed by EDX data showing a strong silicon peak at around 1.75 keV.

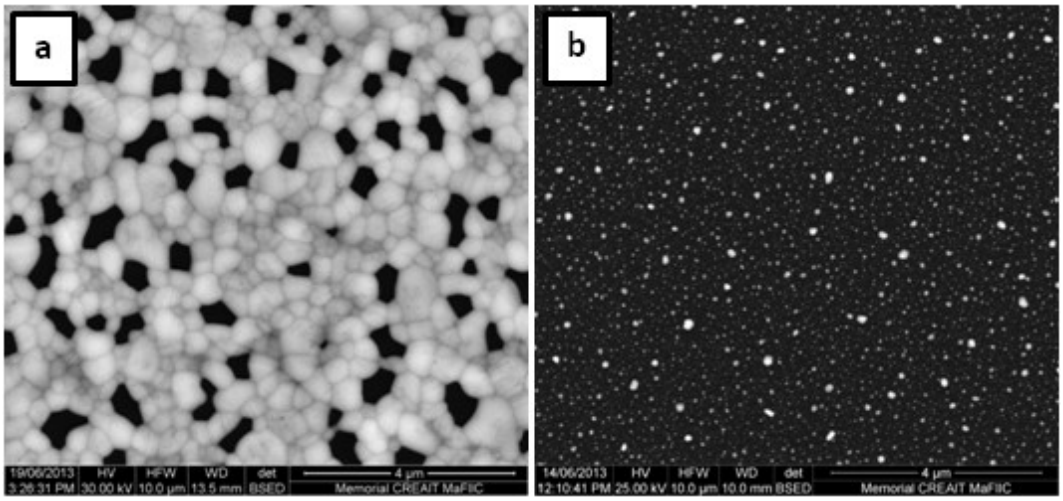

Figure 4.1.4.2: A comparison of SEM images between two different types of bilayers: (a) Au/Ag thin bilayer and (b) Au/Cu bilayer. Both were annealed at 350ºC. In (b), a larger distribution of particles than that of (a) may have caused a weaker SERS response.

Jeon *et al.*[18] observed that surface roughness is one of the key factors that affects SERS enhancement. Generally, SERS enhancement increases with increasing surface roughness.[19,20] The AFM analysis showed that the Au/Cu bilayers had a relatively smaller surface roughness (8.51 nm) compared to the Au/Ag mixed layer (150.46 nm) and Au/Ag bilayers (38.93 nm for the thin bilayer and 45.76 nm for the thick bilayer). Annealing causes bumps that produce larger surface roughness. However, annealing of the Au/Cu bilayer did not cause major changes in the surface features, thereby causing the annealed substrates to have a poor surface roughness. Therefore, a small surface roughness of the Au/Cu bilayers may have caused a weak SERS response to be produced. Furthermore, copper-based substrates are less stable than silver- or gold-based substrates.[13]

4.2 Metal-glass substrates

The glass substrate often influenced the Raman spectrum of the film. For reference, Figure 4.2.1 shows the Raman spectrum of a plain glass slide.

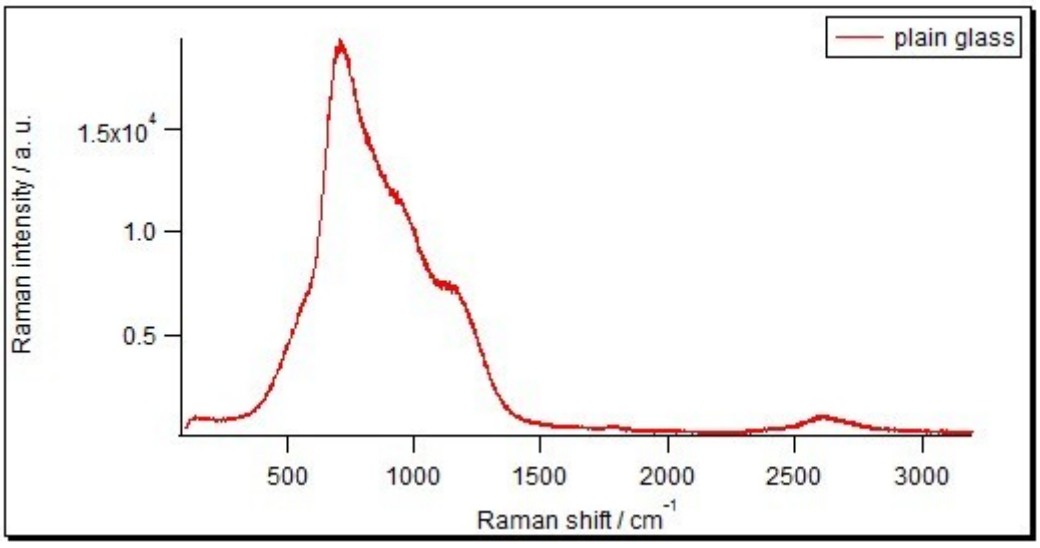

Figure 4.2.1: Reference Raman spectrum of a plain glass slide.

4.2.1 Ag/Cr bilayer

The SERS spectra of the Ag/Cr/glass substrates are shown in Figure 4.2.1.1.

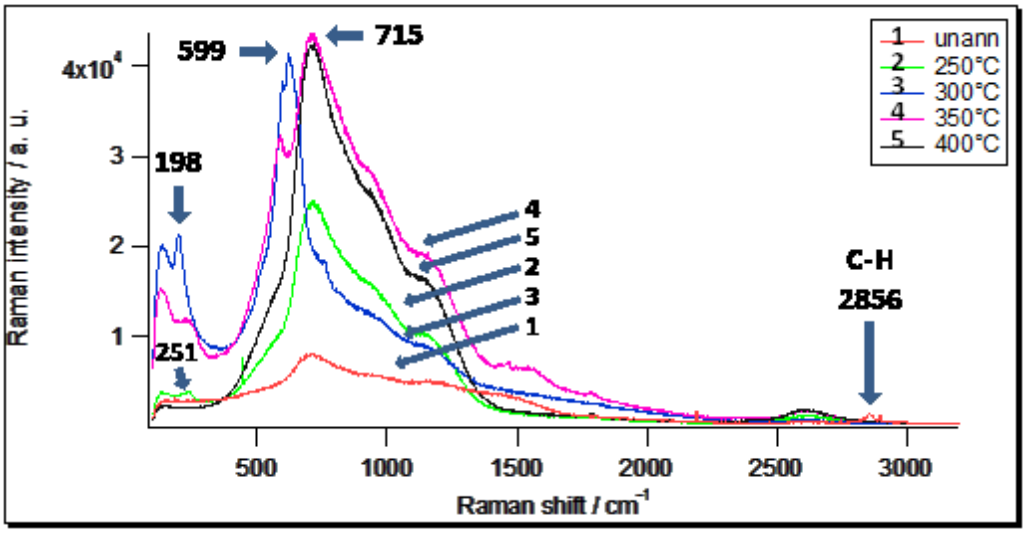

Figure 4.2.1.1: SERS spectra of phenanthrene on a Ag/Cr/glass substrate.

Results

Preannealed substrate: A phenanthrene peak was observed at around 709 cm^{-1}, but its intensity was poor compared to those of the annealed samples. The characteristic aromatic C-H stretching vibrations appeared at 2835, 2856, and 2899 cm^{-1}.[7,21] Preannealed substrate were only slightly affected by background fluorescence.

Substrate annealed at 250°C: Two small bumps were observed at 142 and 251 cm^{-1} and an intense fluorescence peak appeared at 714 cm^{-1}. Also, a small bump is visible at around 2600 cm^{-1}.

Substrate annealed at 300°C: Characteristic phenanthrene peaks were observed at 136, 198, 599, 621, and 752 cm^{-1}. The peak at 599 cm^{-1} was assigned to the in-plane C-C-C deformation[1] and the peak at 752 cm^{-1} was attributed to the skeletal stretching vibrations.[22]

Substrate annealed at 350ºC: Phenanthrene peaks were observed at 131, 231, 590, 715, and 1441 cm^{-1}. The peak at 1441 cm^{-1} was assigned to the C-C stretching vibrations of the aromatic rings.[1] The intense characteristic Raman signal of silver oxide (AgO) was observed at 216 cm^{-1}.[6] Therefore, the peak at 231 cm^{-1} was assumed to occur because of the presence of AgO layers. The centre of the large fluorescence peak is located at 715 cm^{-1}. Peaks with unknown characterization were observed at 1463 and 1538 cm^{-1}.

Substrate annealed at 400ºC: The spectrum was dominated by glass fluorescence with a small bump appeared at 2600 cm^{-1}.

Discussion

The results of the Ag/Cr bilayer samples with aqueous phenanthrene treatment show that the substrate annealed at 300ºC gave the highest SERS enhancement and that the sample annealed at 350ºC gave the second highest. The preannealed sample was the least responsive towards SERS. The region of the surface covered by silver was the most SERS-active.[20] The EDX data showed that the preannealed sample did not have a silver layer thickness that was high enough to produce a strong SERS enhancement. Therefore, we can expect a poor SERS response for the preannealed substrate. More evidence for this conclusion comes from the relatively smaller (20.81 nm) surface roughness for the preannealed sample compared to the annealed samples. On the other hand, the AFM data showed a much larger surface roughness for the samples annealed at 300ºC (53.04 nm) and 350ºC (52.67 nm). The SEM images (Figure 4.2.1.2) show that the sample annealed at 350ºC contained bright spots enriched with silver, but the amounts of silver were

reduced at a higher annealing temperature (400ºC). This may have caused a poor SERS enhancement of the sample annealed at 400ºC. Large SERS enhancement for the samples annealed at 300ºC and 350ºC were believed to be caused by their high surface roughness and high silver content on their surface.

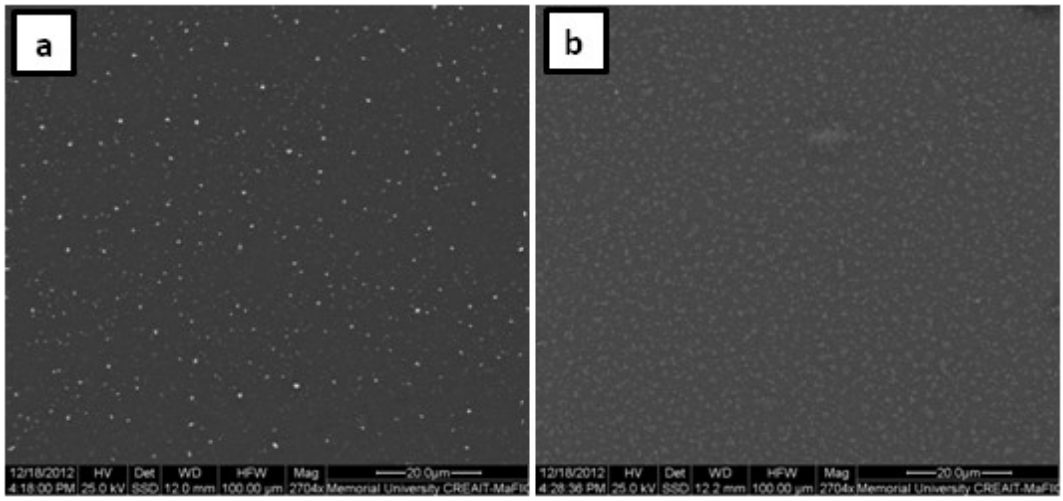

Figure 4.2.1.2: SEM images of the Ag/Cr/glass samples: (a) annealed at 350ºC and (b) annealed at 400ºC. In (a), the spots represent the areas with enriched silver (bright), chromium with less silver (grey), and absence of either silver or chromium (dark). In (b), the apparent absence of silver may have caused a decline in SERS intensity.

Effects of annealing and background fluorescence

One of the most challenging aspects of Raman spectroscopy is the appearance of background fluorescence.[23] It is more pronounced if glass substrates are used. In fact, there is a competition between SERS enhancement and background fluorescence. The Ag/Cr/glass substrates show that annealing increases surface roughness which, in turn, increases the SERS intensity. Also, annealing improves metal bilayer and analyte

contact.[17] This results in more SERS signals being detected for the annealed samples than for the preannealed sample. However, annealing increases background fluorescence when glass substrates are used. Background fluorescence was lowest in the spectra for the preannealed sample and highest in the samples annealed at 350ºC. In the Ag/Cr/glass system, it was observed that annealing displaces the position of the fluorescence peaks. The most intense fluorescence band appeared at 721 cm^{-1} for the sample annealed at 350ºC dropped to 703 cm^{-1} for the preannealed sample. Therefore, it is necessary to address issues relating to background fluorescence when working with glass substrates. Fortunately, fluorescence can be minimized by increasing the time it takes to acquire the Raman image.[1] If this could be done properly, the glass substrates would be a more promising option for the fabrication of optical sensors and biosensors. Furthermore, these cost effective glass materials provide good stability and a small amount of substances can be characterized easily on glass surfaces.[24]

4.3 Metal-acetate substrates

The principal Raman peaks obtained from acetate substrates correspond to the peaks observed in the blank acetate sheet. In most instances, the intense peaks from the acetate sheet were superimposed over the phenanthrene spectrum (Figure 4.3.1). This made it difficult to identify the individual functional groups of phenanthrene.

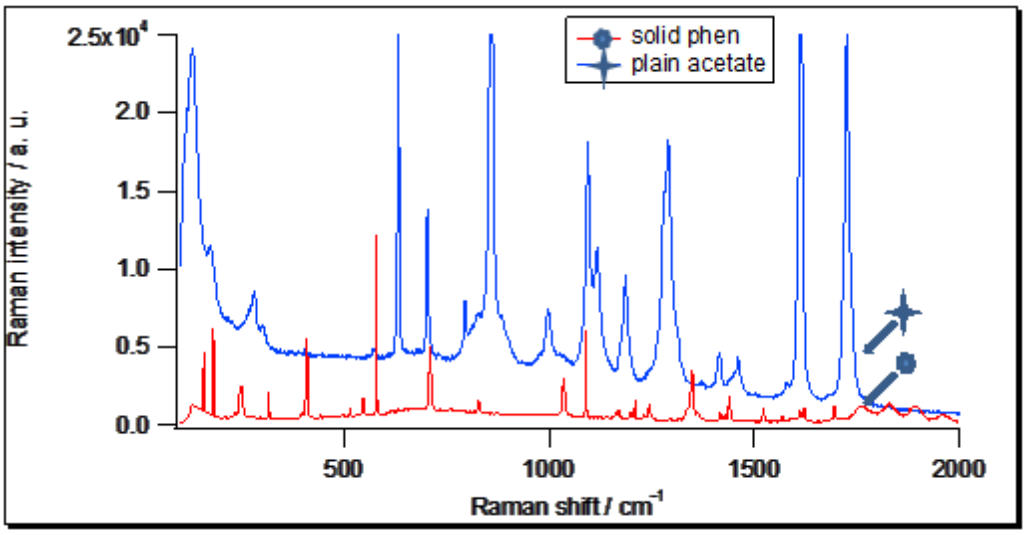

Figure 4.3.1: A comparison of the Raman spectrum of solid phenanthrene with that of the plain acetate sheet.

4.3.1 Cu/acetate

The SERS spectra for the Cu/acetate system are shown in Figure 4.3.1.1.

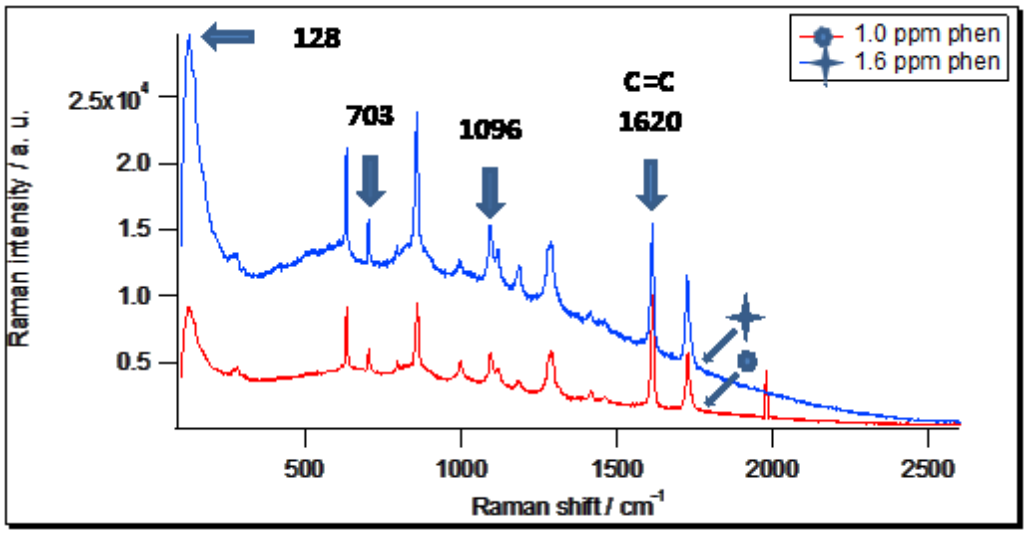

Figure 4.3.1.1: Raman spectra of the Cu/acetate substrate treated with phenanthrene solution. Thick arrows illustrate peaks that were common to both phenanthrene and the acetate sheet.

Results and discussion

The Cu/acetate substrate displayed almost the same number of Raman signals as the plain acetate sheet, but with larger intensities. The substrate exposed to the 1.6 ppm solution of phenanthrene was more heavily influenced by background fluorescence than the substrate exposed to the 1.0 ppm solution. Major Raman peaks corresponding to both phenanthrene and the acetate sheet were observed at 128, 703, 1096, and 1620 cm^{-1}.

4.3.2 Au/Cu/acetate

The SERS spectra of the Au/Cu/acetate system are shown in Figure 4.3.2.1.

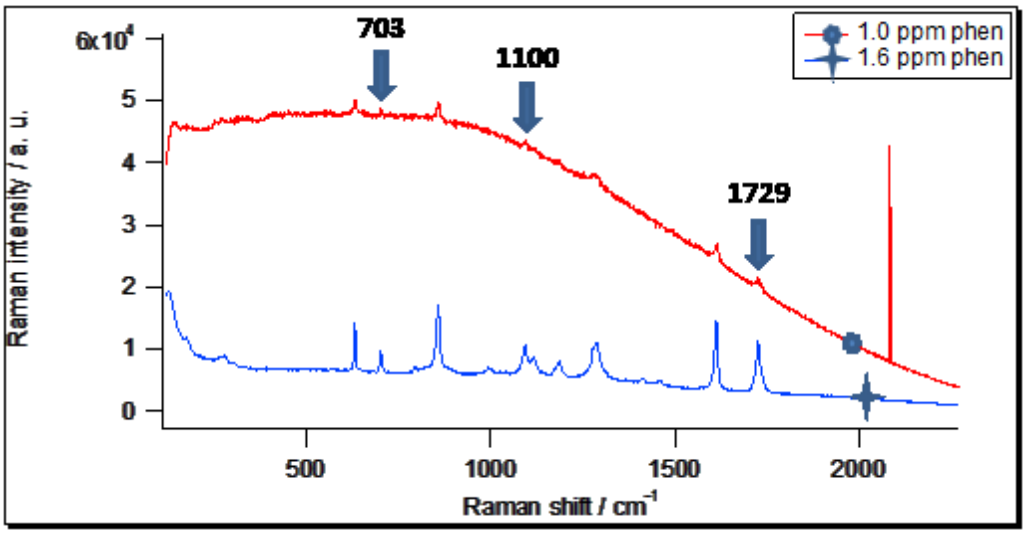

Figure 4.3.2.1: Raman spectra of phenanthrene on a Au/Cu/acetate substrate. The arrows show peaks present in both phenanthrene and the acetate sheet.

Results and discussion

The substrate exposed to the 1.0 ppm solution of phenanthrene was more heavily influenced by background fluorescence than the substrate exposed to the 1.6 ppm solution. The substrate treated with the 1.6 ppm solution produced more signals. Major Raman peaks corresponding to both phenanthrene and the acetate sheet were observed at 703, 1100, and 1729 cm^{-1}.

4.3.3 Ag/acetate

The SERS spectra of the Ag/acetate system are shown in Figure 4.3.3.1.

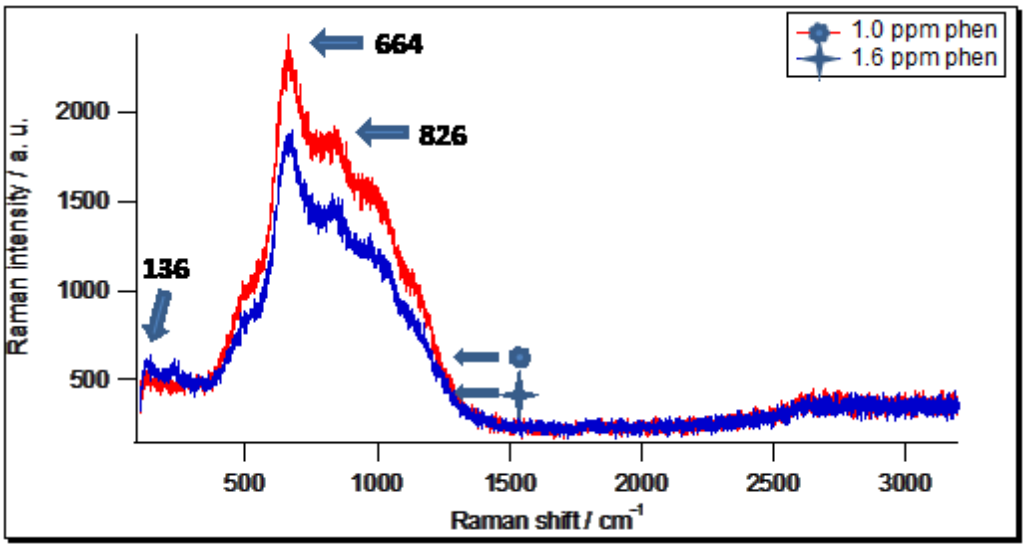

Figure 4.3.3.1: SERS spectra of phenanthrene on a Ag/acetate substrate. The thick arrows, except for the one pointing to the band at 664 cm^{-1}, show the peaks that were caused by phenanthrene (664 cm^{-1} was caused by fluorescence).

Results and discussion

Two shoulders were observed at around 136 and 826 cm^{-1}. They correspond to the solid phenanthrene peaks. Like the Ag/Cr/glass substrates, the SERS spectra for the Ag/acetate systems were heavily influenced by background fluorescence. The position of the highest fluorescence peak of this system was almost identical to the position of the highest fluorescence peak for the Ag/Cr/glass substrates (~700 cm^{-1}).

4.3.4 Au/Ag/acetate

The SERS spectra of the Au/Ag/acetate system are shown in Figure 4.3.4.1.

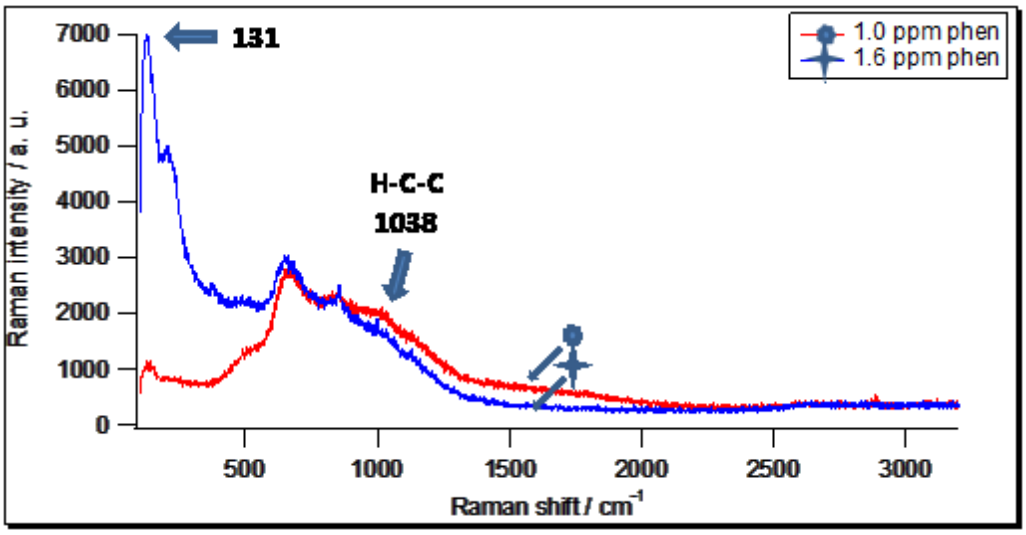

Figure 4.3.4.1: SERS spectra of phenanthrene on a Au/Ag/acetate substrate. The thick arrow corresponds to a phenanthrene peak.

Results and discussion

Characteristic phenanthrene peaks were observed at 131 and 1038 cm^{-1}. The Au/Ag/acetate substrates were heavily influenced by background fluorescence.

4.3.5 Cu/Ag/acetate

The SERS spectra of the Cu/Ag/acetate system are shown in Figure 4.3.5.1.

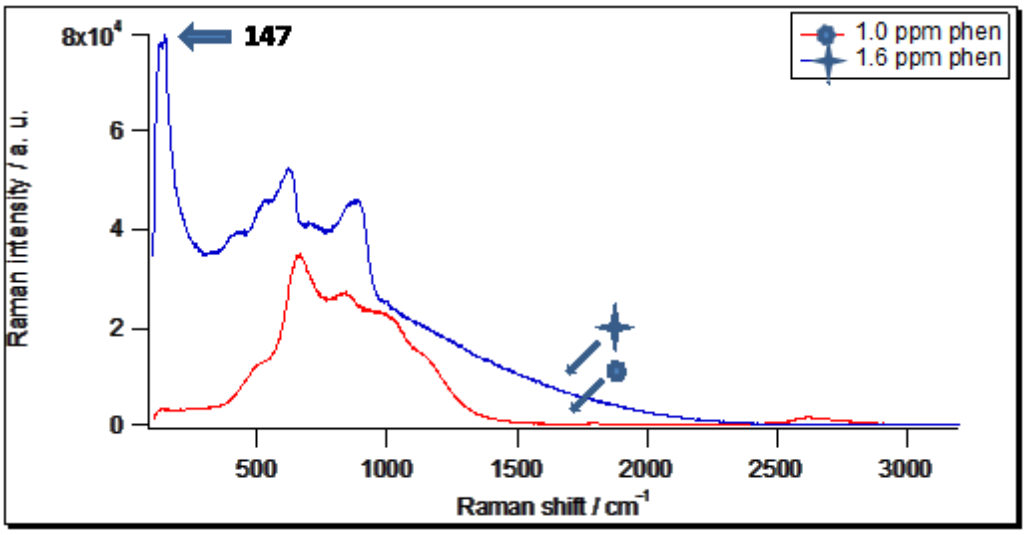

Figure 4.3.5.1: SERS spectra of phenanthrene on a Cu/Ag/acetate substrate. The thick arrow corresponds to a phenanthrene peak.

Results and discussion

No significant spectral features were observed for the Cu/Ag/acetate system. However, an intense peak corresponding to the phenanthrene signal appeared at 147 cm^{-1}. The Cu/Ag/acetate substrates were heavily influenced by background fluorescence like the other substrates partly made up of acetate sheets.

4.4 Drawbacks of the present study

The substrates described in this work were tested in freshwater samples, but the intended application is in seawater. Silver materials are unstable in saline water[25] and copper forms an oxide in the presence of atmospheric oxygen.[13] However, metal oxides can form effective sublayers to enhance SERS from the attached noble metal,[3] therefore subsequent

tests need to be carried out on the SERS activity of these substrates in saline samples. Overall, SERS is considered as an effective tool for the detection of PAHs in screening environmental samples due to its non-invasive nature to target molecues.[14,26,27,28]

Bibliography

[1] Alajtal, A. I.; Edwards, H. G. M.; Elbagerma, M. A.; Scowen, I. J. *Spectrochimica Acta Part A*, **2010**, 76, 1-5.

[2] Alajtal, A. I.; Edwards, H. G. M.; Scowen, I. J. *Anal. Bioanal. Chem.*, **2010**, 397, 215-221.

[3] Shinde, V. V.; Jadhav, P. R.; Kim, J. H.; Patil, P. S. *J. Mater. Sci.*, **2013**, 48, 8393-8401.

[4] Qu, L.-L.; Li, Y.-T.; Li, D.-W.; Xue, J.-Q.; Fossey, J. S.; Long, Y.-T. *Analyst*, **2013**, 138, 1523-1528.

[5] Pristinski, D.; Tan, S.; Erol, M.; Du, H.; Sukhishvili, S. *J. Raman Spectrosc.*, **2006**, 37, 762-770.

[6] Raju, N. R. C.; Kumar, K. J. *J. Raman Spectrosc.*, **2011**, 42, 1505-1509.

[7] Puerto, E. D.; Domingo, C.; Sanchez-Cortes, S.; García-Ramos, J. V.; Aroca, R. F. *J. Phys. Chem. C*, **2011**, 115, 16838-16843.

[8] Marimuthu, A.; Christopher, P.; Linic, S. *J. Phys. Chem. C*, **2012**, 116, 9824-9829.

[9] Shi, X.; Kwon, Y.-H.; Ma, J.; Zheng, R.; Wang, C.; Kronfeldt, H.-D. *J. Raman Spectrosc.*, **2013**, 44, 41-46.

[10] Xie, Y.; Wang, X.; Han, X.; Song, W.; Ruan, W.; Liu, J.; Zhao, B.; Ozaki, Y. *J. Raman Spectrosc.*, **2011**, 42, 945-950.

[11] Fu, C. Y.; Kho, K. W.; Dinish, U. S.; Koh, Z. Y.; Malini, O. *J. Raman Spectrosc.*, **2012**, 43, 977-985.

[12] Prokopec, V.; Cejkova, J.; Matějka, P.; Hasal, P. *Surf. Interface Anal.*, **2008**, 40, 601-607.

[13] Muniz-Miranda, M.; Gellini, C.; Giorgetti, E. *J. Phys. Chem. C*, **2011**, 115, 5021-5027.

[14] Xie, Y.; Wang, X.; Han, X.; Xue, X.; Ji, W.; Qi, Z.; Liu, J.; Zhao, B.; Ozaki, Y. *Analyst*, **2010**, 135, 1389-1394.

[15] Zhu, J.; Li, J.-J.; Yuan, L.; Zhao, J. W. *J. Phys. Chem. C*, **2012**, 116, 11734-11740.

[16] Jain, P. K.; Huang, W.; El-Sayed, M. A. *Nano Lett.*, **2007**, 7(7), 2080-2088.

[17] Xu, W.; Xiao, J.; Chen, Y.; Chen, Y.; Ling, X.; Zhang, J. *Adv. Mater.*, **2013**, 25, 928-933.

[18] Jeon, T. Y.; Park, S.-G.; Lee, S. Y.; Jeon, H. C.; Yang, S.-M. *ACS Appl. Mater. Interfaces*, **2013**, 5, 243-248.

[19] Lin, H.-X.; Li, J.-M.; Liu, B.-J.; Liu, D.-Y.; Liu, J.; Terfort, A.; Xie, Z.-X.; Tian, Z.-Q.; Ren, B. *Phys. Chem. Chem. Phys.*, **2013**, 15, 4130-4135.

[20] Bechelany, M.; Brodard, P.; Philippe, L.; Michler, J. *Nanotech.*, **2009**, 20, 455302 (1-8).

[21] Liu, Y.-L.; Zhou, J.-B.; Zhao, R.-S.; Chen, X.-F. *Anal. Bioanal. Chem.*, **2012**, 404, 1603-1610.

[22] Gabudean, A. M.; Biro, D.; Astilean, S. *Nanotech.*, **2012**, 23, 485706 (1-9).

[23] Smith, E.; Dent, G. *Modern Raman Spectroscopy - A Practical Approach*, **2005**, John Wiley & Sons, p. 1.

[24] Simo, A.; Polte, J.; Pfänder, N.; Vainio, U.; Emmerling, F.; Rademann, K. *J. Am. Chem. Soc.*, **2012**, 134, 18824-18833.

[25] Lucht, S.; Murphy, T.; Schmidt, H., Kronfeld, H.-D. *J. Raman Spectrosc.*, **2000**, 31, 1017-1022.

[26] Sheng, P.; Wu, S.; Bao, L.; Wang, X.; Chen, Z.; Cai, Q. *New J. Chem.*, **2012**, 36, 2501-2505.

[27] Pfannkuche, J.; Lubecki, L.; Schmidt, H.; Kowalewska, G.; Kronfeldt, H.-D. *Marine Pollut. Bullet.*, **2012**, 64, 614-626.

[28] Jiang, X.; Lai, Y.; Yang, M; Yang, H.; Jiang, W.; Zhan, J. *Analyst*, **2012**, 137, 3995-4000.

Chapter 5

Conclusion and future directions

5.1 Summary

The Au/Ag bilayers that were deposited on silicon wafers generated large Raman signals for phenanthrene. The highest annealing temperatures (i.e. 350ºC and 400ºC) reduced the intensity of the signals. Also, a low metal thickness produced larger signals than a high metal thickness. The behaviour of the Au/Ag mixed film was different from that of the bilayer films. While the signals of the bilayer substrates increased upon annealing up to 300ºC, the mixed film showed the most intense signals when it was unannealed. This result is attributed to the formation of well-separated clusters on the mixed film at higher temperatures. Also, Au/Cu thin films deposited on silicon wafers gave a weak SERS response. All in all, these results show that the Au/Ag substrates are excellent devices for the detection of PAHs in bodies of water.

The Ag/Cr bilayer that was deposited on a glass slide generated large Raman signals for phenanthrene. The observed spectra may have been attributed to a combination of the silver content of the top layer and surface roughness. The substrate that was annealed at 300ºC generated the largest Raman signals. The likely cause of this effect was the relatively high surface roughness of the substrate. The amount of silver in the bilayer was

reduced at higher annealing temperatures. This resulted in poorer SERS signals. These results show that it is crucial to take SERS measurements at the annealing temperature that will maximize the size of the Raman signal. Also, they show that inexpensive and easily prepared silver-glass substrates can be used in the future to develop portable SERS sensors that detect PAHs in water.

The performance of the metal-acetate substrates was poor. The Raman signals generated by the analyte were masked by those of the blank acetate sheet. As a result, the characterization of individual analyte signals was very difficult. This result shows that metal-acetate sheets are not reliable SERS substrates.

5.2 Future directions

SERS is an excellent tool to identify PAHs in bodies of water because it is non-destructive and wieldy. However, the poor reproducibility,[1] but high sensitivity[1] of SERS spectra makes the technique a 'double-edged' sword.[2] Therefore, it demands a thorough study on the sensitivity and reproducibility behaviors of SERS technique in detecting PAHs from aqueous phase using metal substrates.

There are several additional parameters which need to be tested as well. The SERS signals will be more intense if silver is deposited on glass and silicon surfaces that have a small thickness (i.e. 2 to 20 nm). Future experiments should be carried out with higher acquisition times and increased light power. Moreover, the performance of these SERS substrates should be studied in experimental set-ups that vary parameters such as excitation wavelength and duration of phenanthrene treatment. Field trials on the

substrates with real environmental samples could be an excellent option to test their efficiency.

Bibliography

1. Fang, J.; Lebedkin, S.; Yang, S.; Hahn, H. *Chem. Commun.*, **2011**, 47, 5157-5159.
2. Xu, W.; Xiao, J.; Chen, Y.; Chen, Y.; Ling, X.; Zhang, J. *Adv. Mater.*, **2013**, 25, 928-933.